Molecular and Cellular Biochemistry Faculty Publications

Molecular and Cellular Biochemistry

Peptide Inhibitors Targeting the *Neisseria gonorrhoeae* Pivotal Anaerobic Respiration Factor AniA

Aleksandra E. Sikora
Oregon State University

Robert H. Mills
Oregon State University

Jacob V. Weber
Oregon State University

Adel Hamza
University of Kentucky

Bryan W. Passow
Oregon State University

See next page for additional authors

Authors

Aleksandra E. Sikora, Robert H. Mills, Jacob V. Weber, Adel Hamza, Bryan W. Passow, Andrew Romaine, Zachary A. Williamson, Robert W. Reed, Ryszard A. Zielke, and Konstantin V. Korotkov

Peptide Inhibitors Targeting the *Neisseria gonorrhoeae* **Pivotal Anaerobic Respiration Factor AniA**

Peptide Inhibitors Targeting the *Neisseria gonorrhoeae* Pivotal Anaerobic Respiration Factor AniA

🆔 Aleksandra E. Sikora,[a] Robert H. Mills,[a] Jacob V. Weber,[a] Adel Hamza,[b*]
Bryan W. Passow,[a] Andrew Romaine,[a] Zachary A. Williamson,[b] Robert W. Reed,[b]
Ryszard A. Zielke,[a] Konstantin V. Korotkov[b]

Department of Pharmaceutical Sciences, College of Pharmacy, Oregon State University, Corvallis, Oregon, USA[a]; Department of Molecular & Cellular Biochemistry, College of Medicine, University of Kentucky, Lexington, Kentucky, USA[b]

ABSTRACT *Neisseria gonorrhoeae* causes the sexually transmitted infection gonorrhea, which is highly prevalent worldwide and has a major impact on reproductive and neonatal health. The superbug status of *N. gonorrhoeae* necessitates the development of drugs with different mechanisms of action. Here, we focused on targeting the nitrite reductase AniA, which is a pivotal component of *N. gonorrhoeae* anaerobic respiration and biofilm formation. Our studies showed that gonococci expressing AniA containing the altered catalytic residues D137A and H280A failed to grow under anaerobic conditions, demonstrating that the nitrite reductase function is essential. To facilitate the pharmacological targeting of AniA, new crystal structures of AniA were refined to 1.90-Å and 2.35-Å resolutions, and a phage display approach with libraries expressing randomized linear dodecameric peptides or heptameric peptides flanked by a pair of cysteine residues was utilized. Biopanning experiments led to the identification of 29 unique peptides, with 1 of them, C7-3, being identified multiple times. Evaluation of their ability to interact with AniA using enzyme-linked immunosorbent assay and computational docking studies revealed that C7-3 was the most promising inhibitor, binding near the type 2 copper site of the enzyme, which is responsible for interaction with nitrite. Subsequent enzymatic assays and biolayer interferometry with a synthetic C7-3 and its derivatives, C7-3m1 and C7-3m2, demonstrated potent inhibition of AniA. Finally, the MIC_{50} value of C7-3 and C7-3m2 against anaerobically grown *N. gonorrhoeae* was 0.6 mM. We present the first peptide inhibitors of AniA, an enzyme that should be further exploited for antigonococcal drug development.

KEYWORDS *Neisseria gonorrhoeae*, anaerobic respiration, AniA, nitrite reductase, phage display, peptide inhibitors, crystal structure, docking studies, biolayer interferometry

Among the human-colonizing *Neisseria* species, only *Neisseria gonorrhoeae*, the causative agent of gonorrhea, is always considered pathogenic. Gonorrhea remains a serious public health concern, with 78 million new cases occurring annually worldwide; has severe consequences on reproductive and neonatal health; and contributes to the transmission and acquisition of HIV (1, 2). Untreated or inadequately treated infections can result in endometritis, pelvic inflammatory disease, ectopic pregnancy, epididymitis, and infertility (3–5). During pregnancy, gonorrhea may lead to chorioamnionitis, which can be further complicated by septic abortion, premature rupture of membranes, and preterm delivery (6). Infants born to infected mothers have an increased risk of ophthalmia neonatorum, which can lead to blindness. There is a pressing need for the development of new antibiotics, improved antibiotic surveillance

strategies, and a gonorrhea vaccine, as *N. gonorrhoeae* strains resistant to the last effective treatment options are emerging and clinical treatment failures have been documented (7–15).

N. gonorrhoeae, initially considered an obligate aerobic bacterium, survives and proliferates in a milieu of obligate anaerobes within the genitourinary tract (16). Pioneering work by Short et al. (17) demonstrated that various gonococci, including laboratory strains and fresh clinical isolates, remained viable during anaerobic inoculation. Subsequently, nitrite was identified to be the critical terminal electron acceptor supporting *N. gonorrhoeae* growth under oxygen-limited conditions (18). Mounting evidence demonstrates that the anaerobic lifestyle is an important state during infection and the stimulon for anaerobic growth comprises about 10% of the *N. gonorrhoeae* genome (19–22). *N. gonorrhoeae* favors anaerobic respiration during growth in biofilms (21–23). Bacteria in biofilms display increased resistance to antimicrobials and host defense mechanisms, and naturally occurring *N. gonorrhoeae* biofilms are linked with persistent infections in women (23–26). Anaerobic growth is accomplished by the utilization of a two-step denitrification pathway consisting of AniA (NGO1276), a copper-containing enzyme that reduces nitrite to nitric oxide, which is subsequently reduced to nitrous oxide by NorB (NGO1275) (Fig. 1). The denitrification pathway is truncated, as it lacks a nitrous oxide reductase complex (27–30). AniA (formerly Pan 1), also known as NirK, is a surface-exposed glycosylated lipoprotein essential for *N. gonorrhoeae* viability under oxygen-limited conditions and enhances gonococcal survival upon exposure to normal human serum (21, 22, 31). Nitrite reductase, in addition to Ccp, cytochrome *c*′, and Laz, provides pathogenic *Neisseria* strains with protection against assaults from reactive oxygen and nitrogen species (32, 33). Further, antibodies to AniA have been found in serum from infected women, demonstrating that *aniA* is expressed *in vivo* (18, 34). For these reasons, interest in AniA's potential as a gonorrhea vaccine candidate has increased recently (31, 35).

In this paper, we propose AniA as a target for pharmacological intervention against gonorrhea. The pharmacological inhibition of AniA should reduce the fitness of the gonococcus in the genital tract, where oxygen tension is reduced, and should augment the ability of existing antimicrobials to clear the pathogen. To facilitate the targeting of AniA with small-molecule inhibitors, we solved new crystal structures of AniA. Subsequently, a phage display approach with highly diversified libraries expressing randomized linear dodecameric peptides or heptameric peptides was utilized to identify peptide ligands interacting with a purified recombinant version of the *N. gonorrhoeae* FA1090 nitrite reductase. These experiments enabled the discovery of 29 unique peptides, with 1 of them, C7-3, being identified multiple times. Evaluation of their ability to interact with AniA using an enzyme-linked immunosorbent assay (ELISA) and computational docking established C7-3 as the most promising inhibitor, binding near the type 2 copper site of the enzyme. Subsequent enzymatic assays with purified AniA, whole-cell nitrite utilization studies, biolayer interferometry (BLI), and MIC_{50} determination demonstrated that synthetic C7-3 and its derivatives have an inhibitory effect on AniA nitrite reductase activity and on *N. gonorrhoeae* growth under anaerobic conditions.

RESULTS

Refining the *N. gonorrhoeae* AniA structure. The structure of *N. gonorrhoeae* AniA has been reported (27). However, the high ionic strength under the crystallization condition of AniA in space group P1 (27) is not readily suitable for cocrystallization with inhibitors. To facilitate the targeting of AniA with small-molecule inhibitors, the recombinant version of AniA, sAniA (36), from *N. gonorrhoeae* strain FA1090 was purified and the new structures of the *N. gonorrhoeae* AniA were solved and refined to 1.90-Å and 2.35-Å resolutions in two novel crystal forms, $P2_12_12_1$ and $I4_122$, respectively (Table 1 and Fig. 1B to D). While the crystals belonging to the $P2_12_12_1$ form were grown under the high-ionic-strength condition, the crystals belonging to the $I4_122$ form were obtained using 0.2 M potassium thiocyanate and 20% polyethylene glycol (PEG) 3350
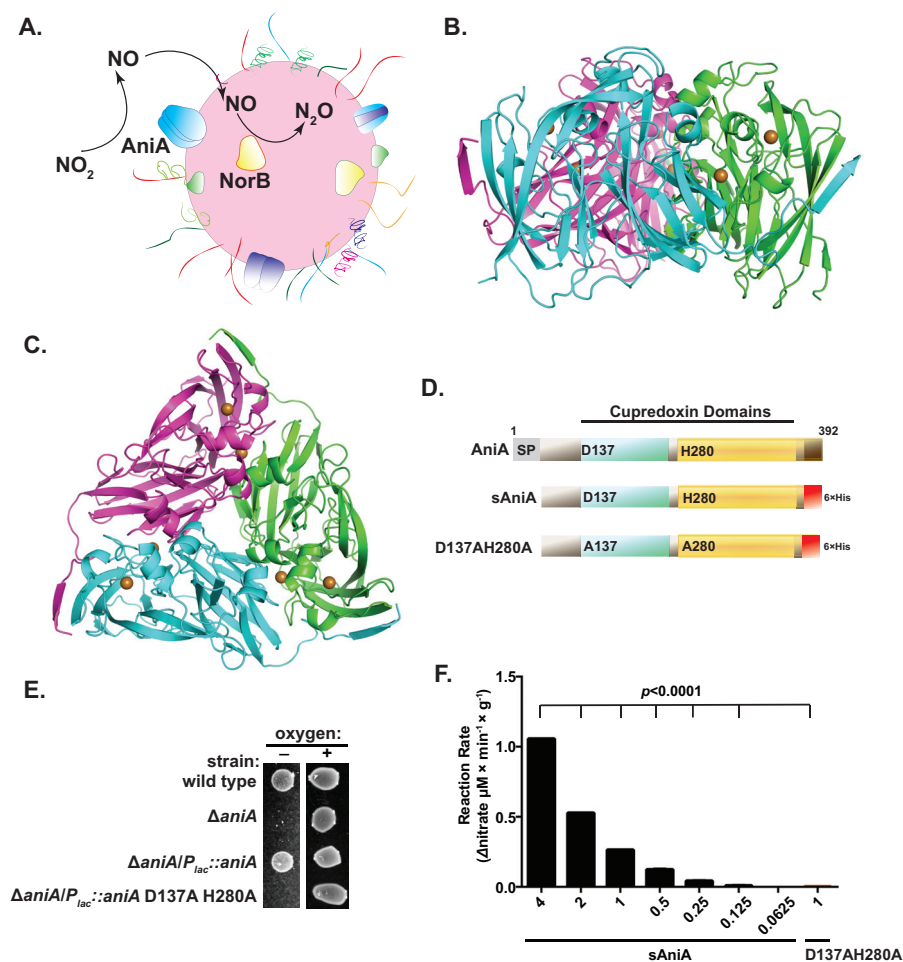
FIG 1 Structural and functional analysis of AniA. (A) Schematic illustration of AniA function in the *Neisseria gonorrhoeae* denitrification pathway. A two-step denitrification pathway in *N. gonorrhoeae* is comprised of AniA (NGO1276), which reduces nitrite to nitric oxide, and NorB, which subsequently reduces nitric oxide to nitrous oxide. (B, C) The crystal structure of the AniA trimer shown in ribbon representation with three subunits colored in green, magenta, and cyan. Side (B) and top (C) views are shown. Each monomer contains two Cu^{2+} ions, shown as gold spheres. (D) Diagram of native AniA and the recombinant variant proteins sAniA and mutated AniA D137A H280A. Gray, signal peptide (SP), amino acids 1 to 20; green, N-terminal cupredoxin domain, amino acids 102 to 198; yellow, C-terminal cupredoxin domain, amino acids 205 to 348; red, the C-terminal 6× His tag. The active-site residues aspartate (D137) and histidine (H280) are also shown. (E) Effect of genetic inactivation of *aniA* and point mutations D137A and H280A on *N. gonorrhoeae* survival under anoxia. Wild-type (wt) strain FA1090, the isogenic knockout Δ*aniA* strain, the complemented Δ*aniA*/P$_{lac}$::*aniA* strain, and the Δ*aniA* strain carrying a mutated version of AniA, Δ*aniA*/P$_{lac}$::*aniA* D137A H280A, were grown in broth to an OD_{600} of 0.2, serially diluted, and spotted onto solid medium supplemented with nitrite and 0.1 mM IPTG. Growth was examined after 22 and 48 h of incubation under aerobic and anaerobic conditions, respectively. (F) Measurements of the nitrite reductase activity of AniA obtained using a fluorometric 2,3-diaminophtalene (DAN) assay. The consumption of nitrite was examined at 37°C under anaerobic conditions in a solution containing sodium nitrite, methyl viologen, sodium dithionate, Tris-HCl, pH 7.0, and either decreasing concentrations of sAniA (in micromolar, as indicated) or AniA D137A H280A (1 μM). The data show the mean reaction rates with the associated SEMs ($n = 10$).

crystallization solution. Therefore, the I4$_1$22 crystals should be readily amenable for cocrystallization or soaking experiments with potential inhibitors or small-molecule fragments. C-terminal residues 355 to 363, which were not modeled in the previous AniA structure (27), form an additional β-strand that reaches over to the neighboring subunit and engages in intersubunit β-strand complementation. Interestingly, similar intersubunit interactions have been observed in the structures of other bacterial nitrite reductases, for example, those from *Alcaligenes faecalis* (37), *Achromobacter xylosoxidans* (38), and *Achromobacter cycloclastes* (39). Otherwise, our AniA structures are

TABLE 1 Data collection and refinement statistics

Parameter[a]	Value(s) for AniA with PDB accession no.[b]:	
	5TB7	**5UE6**
Data collection statistics		
Wavelength (Å)	1.0000	1.0000
Space group	$P2_12_12_1$	$I4_122$
Unit cell dimensions		
a, b, c (Å)	76.23, 129.10, 136.72	177.34, 177.34, 449.46
α, β, γ (°)	90, 90, 90	90, 90, 90
Resolution (Å)	66.58–1.90 (1.95–1.90)	83.68–2.35 (2.41–2.35)
R_{sym}	0.090 (1.038)	0.179 (1.050)
$CC_{1/2}$	99.8 (67.7)	99.0 (75.4)
$I/\sigma I$	11.7 (1.9)	5.8 (1.8)
Completeness (%)	99.2 (100)	84.8 (83.3)
Multiplicity	6.2 (6.3)	4.2 (3.9)
Refinement statistics		
Resolution (Å)	66.58–1.90	83.68–2.35
No. of reflections (total/free)	105,946/10,240	125,511/11,871
R_{work}/R_{free}	0.155/0.179	0.236/0.259
No. of atoms		
Protein	7,156	21,242
Ligand/ion	21	27
Water	486	984
B factors		
Protein	34.1	37.2
Ligand/ion	53.7	36.5
Water	41.9	32.2
All atoms	34.6	36.1
Wilson B	37.4	31.7
RMSD		
Bond lengths (Å)	0.010	0.003
Bond angles (°)	1.006	0.638
Ramachandran distribution[c] (%)		
Favored	98.7	98.2
Outliers	0	0
MolProbity score[d]	0.71	0.79

[a]$CC_{1/2}$, correlation coefficient, as defined in the work of Karplus and Diederichs (101) and calculated by XSCALE (102); I, intensity of a reflection; RMSD, root mean square deviation.
[b]Values in parentheses are for the highest-resolution shell.
[c]Calculated using the MolProbity server (http://molprobity.biochem.duke.edu) (73).
[d]MolProbity score combines the clash score, rotamer, and Ramachandran evaluations into a single score, normalized to be on the same scale as the X-ray resolution (73).

similar to the previously determined AniA structure (27), with the root mean square error between individual subunits being 0.3 Å (Fig. 1B and C).

   N. gonorrhoeae AniA is a trimer, with each monomer consisting of two β-sandwich cupredoxin domains (Fig. 1). The monomers contain two types of Cu-binding sites involved in catalysis. The type 1 Cu site is coordinated by the Cys125, Met188, His134, and His183 residues from the same subunit. The type 2 Cu site is located on the interface between subunits and is coordinated by His139 and His174 residues from one subunit and a His329 residue from another subunit. Interestingly, another His residue, His280, is located in the vicinity of the type 2 Cu site but does not directly coordinate the Cu ion.

   The nitrite reductase function of AniA is pivotal for *N. gonorrhoeae* survival under anaerobic conditions. An insertional mutation within the *aniA* locus caused the loss of *N. gonorrhoeae* viability under anaerobic growth conditions (28, 40). Corroborating these findings, a strain with an in-frame *aniA* deletion knockout in the FA1090 background, the Δ*aniA* strain, grew robustly aerobically, but no colonies were observed under oxygen-limited conditions (Fig. 1E). To test whether this effect on gonococcal viability was associated with the nitrite reductase function of AniA, a mutated version of the enzyme with altered predicted catalytic residues D137A and H280A (Fig. 1) (27) was created using site-directed mutagenesis. Subsequently, the wild-type (wt) *aniA*

allele and the *aniA* D137A H280A allele were cloned under the control of the P$_{lac}$ promoter and introduced individually into the chromosome of FA1090 Δ*aniA*, creating the Δ*aniA*/P$_{lac}$::*aniA* and Δ*aniA*/P$_{lac}$::*aniA* D137A H280A strains, respectively. Bacterial suspensions of the same optical density were spotted on gonococcal base solid medium (GCB) containing nitrite as a terminal electron acceptor and IPTG (isopropyl-β-D-thiogalactopyranoside) to induce expression of *aniA*. Under aerobic conditions, all strains grew similarly to wild-type *N. gonorrhoeae*, and full complementation of the Δ*aniA* phenotype was achieved in the Δ*aniA*/P$_{lac}$::*aniA* strain incubated anaerobically. In contrast, the Δ*aniA*/P$_{lac}$::*aniA* D137A H280A strain failed to form colonies under oxygen-limited conditions, demonstrating that the nitrite reductase function of AniA is critical for *N. gonorrhoeae* survival during anaerobiosis (Fig. 1E). To assess the enzymatic activities of sAniA and AniA D137A H280A, both recombinant proteins were purified in milligram quantities to homogeneity (see Fig. S1 in the supplemental material) and nitrite utilization was measured in a fluorometric assay (27, 41–43). The enzymes were individually incubated with nitrite as the substrate and dithionate-reduced methyl viologen as an artificial electron donor. Following incubation, the reactions were stopped and the concentrations of residual nitrite were determined with the 2,3-diaminonaphthalene (DAN) reagent (42). As shown in Fig. 1F, the wild-type protein, sAniA, consumed nitrite in a dose-dependent manner, whereas the mutated version of AniA, AniA D137A H280A, displayed completely abolished nitrite reductase activity.

Together, the results of these studies demonstrate the importance of the predicted catalytic residues D137 and H280 in the enzymatic function of AniA and gonococci viability under anoxia.

AniA is expressed in a panel of geographically, temporally, and genetically diverse gonococcal isolates. AniA appeared as one of the major anaerobically induced outer membrane proteins that was not detected under aerobic growth (44, 45). We, however, have shown that four different laboratory isolates of *N. gonorrhoeae* cultured under standard aerobic conditions, as well as in the presence of normal human serum and during iron deprivation, had sufficient amounts of AniA to be detectable not only by mass spectrometry but also by standard immunoblotting (36, 44). Analysis of *aniA* conservation (Fig. S2) demonstrated the existence of 318 alleles with 395 single nucleotide polymorphic sites present in 42,088 isolates of *Neisseria* spp. deposited into the PubMLST database (http://pubmlst.org/neisseria/, as of 25 January 2017). Further, expression of *aniA* was tested in whole-cell lysates derived from 36 aerobically grown different *N. gonorrhoeae* strains isolated from patients at different times and from different geographic locations, including the 2016 WHO reference strains (46), by SDS-PAGE and immunoblotting with polyclonal anti-AniA antiserum (36). Antiserum against AniA cross-reacted with all clinical isolates, albeit with noticeable differences in AniA levels being found between the strains (Fig. 2).

The conservation and expression of AniA under different growth conditions and among diverse gonococcal isolates further highlight the importance of maintaining this outer membrane protein in *N. gonorrhoeae*.

Targeting AniA using a phage display approach. We chose a phage display approach to identify peptide ligands interacting with AniA, as this technology has been successfully applied in basic and translational research and some of the identified peptides are currently in preclinical or clinical trials (47, 48). To provide a high diversity of peptide sequences, two commercially available M13 phage-based randomized peptide libraries comprised of 1.9×10^9 independent linear dodecameric peptides (Ph.D.-12) and 3.7×10^9 heptameric peptides each flanked by a pair of cysteine residues (Ph.D.-C7C) were used (Fig. 3). We utilized an affinity capture method by immobilizing sAniA onto magnetic Ni-nitrilotriacetic acid (NTA) agarose and, as outlined in Fig. 3, preclearing steps prior to each biopanning experiment to remove Ni-NTA- and plastic-binding sequences. Additionally, increasing stringency was applied during the wash steps of three consecutive rounds of the biopanning experiments. Finally, the DNA of 24 randomly chosen phages from each group was extracted and sequenced. A total of
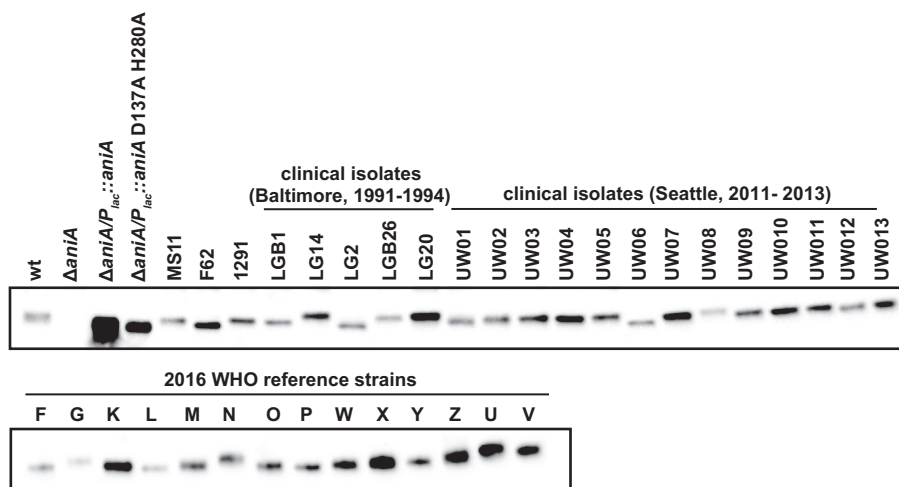
FIG 2 AniA is expressed in a diverse panel of *N. gonorrhoeae* isolates. *N. gonorrhoeae* wild-type strain FA1090, the isogenic Δ*aniA*/P*lac*::*aniA* strain, and the Δ*aniA*/P*lac*::*aniA* D137A H280A strain, as well as 36 additional strains of *N. gonorrhoeae*, as indicated above the immunoblots, were grown concurrently on solid medium for 20 h in 5% CO_2 at 37°C. The Δ*aniA*/P*lac*::*aniA* and Δ*aniA*/P*lac*::*aniA* D137A H280A strains were grown on solid medium supplemented with IPTG. Samples containing the whole-cell lysates were matched by equivalent OD_{600} units, resolved in a 4 to 20% Tris-glycine gel, and transferred onto nitrocellulose. The immunoblotting was performed using polyclonal rabbit antiserum against sAniA.

29 different deduced peptide sequences were identified, with 6 and 23 different peptides being identified in the Ph.D.-C7C and Ph.D.-12 phage pools, respectively. Strikingly, one heptameric peptide, designated C7-3 (CNYCRLNLW), was identified 19 times (Fig. 3B).

The ability of the phage-displayed peptides to bind to sAniA was subsequently examined in a monoclonal phage enzyme-linked immunosorbent assay (ELISA). The 29 phage clones, 10^{10} PFU per well, were individually incubated in microtiter plates coated with sAniA. Following extensive washing, the signal was detected by a monoclonal anti-M13–horseradish peroxidase (HRP) conjugate coupled with a colorimetric reaction (Fig. 3C). These studies revealed C7-3 and 12-5 (KHYYGGDTTTLW) to be the best binding among the heptameric and dodecameric phage-expressed peptides, respectively, and these two peptides were selected for further investigation.

Docking studies. It has been observed that normal mode analysis (NMA) is well suited for describing conformational changes between bound and unbound (apo-form) protein structures (49–51). To understand AniA-peptide interactions, it was critical to determine the flexibility and the conformational states of the homotrimer AniA structure. Whereas in the standard molecular dynamics (MD) simulation all atoms of the protein are of equal importance, in our approach we considered that the structural flexibility of the protein conformation is better represented by the linear combinations of the lowest normal modes of vibrations. Thus, we approximated the total molecular flexibility by considering only the most significant degrees of freedom (50, 51). As shown in Fig. 4, the motion of the four combined lowest normal modes of vibrations described the opening and closing states of cupredoxin domain II (Cu^{2+} catalytic active site) of the AniA structure. Thus, NMA revealed the tendency of the protein to move in a certain direction, even though this movement was not fully explored during the MD simulations.

The view of the top of the catalytic active site of the AniA structure (Fig. 4) shows that the flexibility of the protein is well oriented and can dramatically change the accessible area of the catalytic metal ion Cu^{2+} and its potential interaction with a ligand (NO_2 or peptide). The open conformation of the homotrimer AniA structure was used to identify several binding pockets.

Prediction of interactions between the C7-3 and 12-5 peptides and AniA. The multiconformational states of the peptides C7-3 and 12-5 were first generated, and the

A.

B.

Ph.D.-C7C

1. CRSTLQHSC
2. CLKNQSDQC
3. CNYCRLNLW
4. CNYCRLNLW
5. CNYCRLNLW
6. CNYCRLNLW
7. CNYCRLNLW
8. CNYCRLNLW
9. CSTSSRTGC
10. CMHVRHGLC
11. CNYCRLNLW
12. CNYCRLNLW
13. CNYCRLNLW
14. CNYCRLNLW
15. CNYCRLNLW
16. CNYCRLNLW
17. CNYCRLNLW
18. CNYCRLNLW
19. CNYCRLNLW
20. CDSAPTRKC
21. CNYCRLNLW
22. CNYCRLNLW
23. CNYCRLNLW
24. CNYCRLNLW

Ph.D.-12

1. HLNHNDNYLPP
2. AYSDRIPSLWDT
3. GYIERGLALWNS
4. YNFDVWKDHWIY
5. KHYYGGDTTTLW
6. SYNFDLWSFGLE
7. HYDRGNLWFQKS
8. GYKVPLWSKPEY
9. AQYERFDWASWW
10. YPSTLREMFWH
11. THDFSKARLWPS
12. EYSSFRLWNIYT
13. YHDLNLWELNVR
14. YHPNGMNPYTKA
15. DYSKMRLWDLRP
16. SYKYPLWHSITL
17. SLSPHYMNLWNA
18. YTGRAIDLWTEW
19. AYPPNLWQKALA
20. AYPPNLWQKALA
21. QYPYDLWSSMQR
22. SMSYKDREMQMW
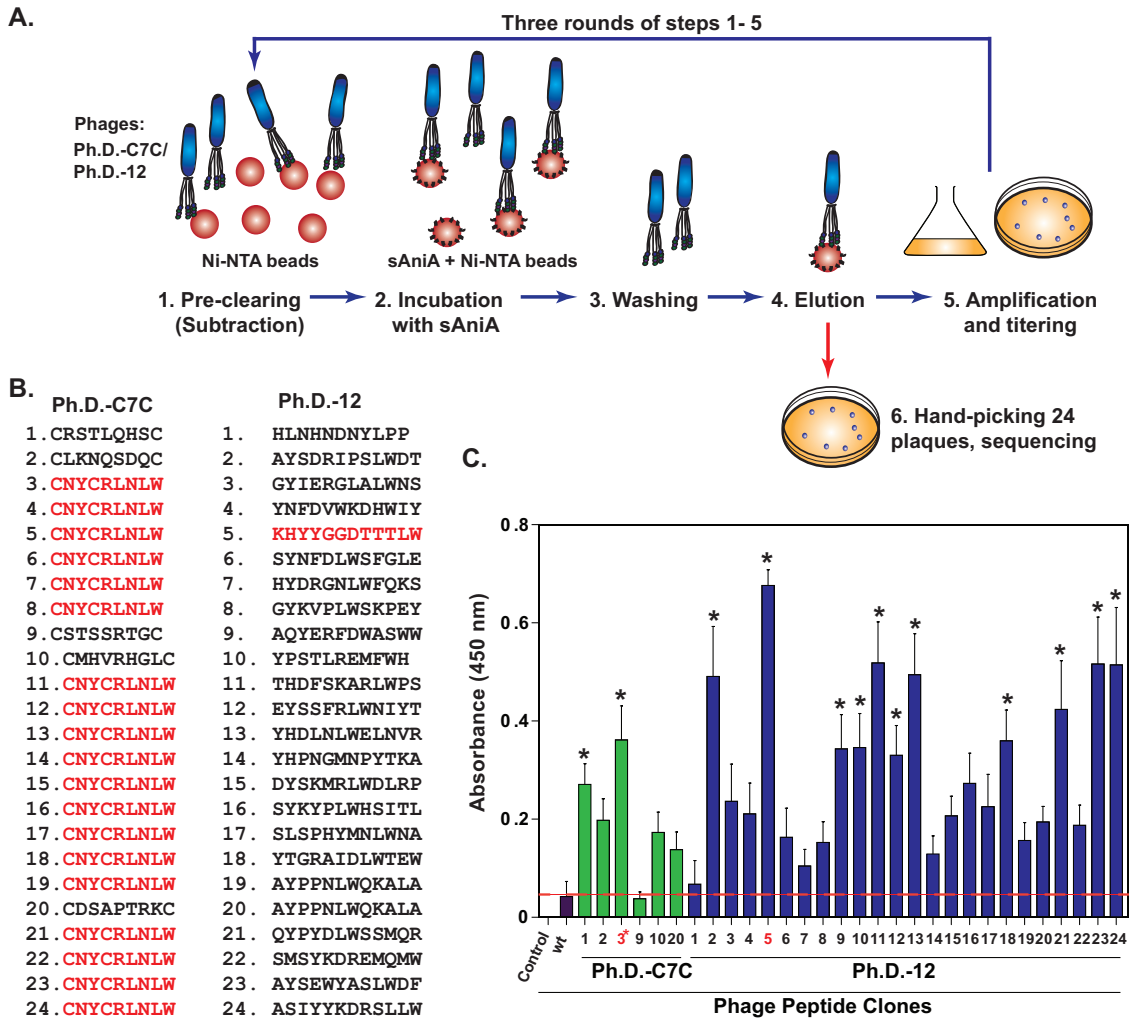23. AYSEWYASLWDF
24. ASIYYKDRSLLW

C.

FIG 3 Targeting AniA using a phage display approach. (A) The recombinant version of AniA, sAniA, was purified to homogeneity and used in an affinity capture method as the bait during three panning experiments with two phage display libraries expressing either randomized linear 12-mer peptides (Ph.D.-12) or randomized 7-mer peptides flanked by a pair of cysteine residues (Ph.D.-C7C). As a first step in every round of the panning experiment, both peptide libraries were precleared against Ni-NTA magnetic chitin resin to remove nonspecifically binding peptides. The supernatants from this step were then added to 200 μg of sAniA bound to the resin. After incubation with the protein, unbound phages were washed away using TBST, with an increasing stringency of the washing being used in consecutive rounds. The elutions were performed with glycine-HCl (pH 2.2). (B) Deduced peptide sequences of the 7-mer and 12-mer peptides obtained by sequencing of the DNA of 24 randomly selected phages from each group eluted after the third round of biopanning. These studies revealed 26 unique peptides, with 1 of them, C7-3, being identified multiple times. Synthesized peptides are shown in red. (C) Evaluation of the identified peptides through phage ELISA. Phage clones were purified and tested separately to measure their affinity to sAniA in the phage ELISA. Purified sAniA (2 μM) was coated overnight at 4°C on 96-well flat-bottom plates. After the coating step, unbound sAniA was removed and the wells were thoroughly washed with the storage buffer. The wells were blocked and incubated with 10^{10} PFU per well from each amplification. After washing, the anti-M13 monoclonal antisera coupled to horseradish peroxidase were added. Unbound antisera were removed by excessive washing, and enzymatic activity was exerted by the addition of Turbo TMB-ELISA substrate. The absorbance at 450 nm was measured. Readings were compared to those of wells which underwent an identical treatment but lacked sAniA (control) and to the signal from a wild-type phage, M13KE (10^{10} PFU), that did not display peptides (wild type). The means and SEMs from seven independent experiments are shown. Clones 3* and 5 (in red) were identified multiple times. *, $P < 0.05$.

conformations of the peptides with the lowest total energy were positioned on top of each cavity with an arbitrary distance of ~8 Å. The AniA-peptide complexes were simulated by MD in a vacuum for 500 ps, and the last 20 final snapshots from the trajectory were used to compute the binding free energy (ΔG_{bind}). The stabilized peptide conformation with the higher binding energy was used for the docking procedure, as described in Materials and Methods. We docked the peptides in the opened Cu^{2+} catalytic active site of the AniA structure. After several docking trials, we
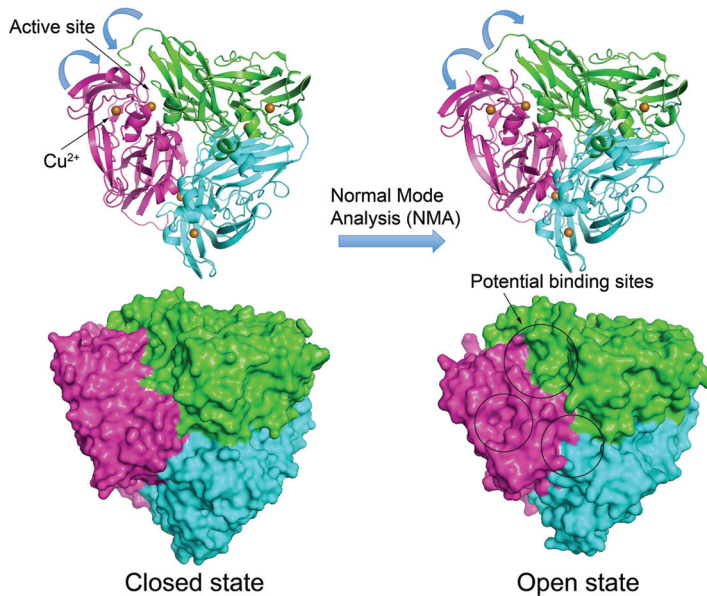
FIG 4 Normal mode analysis (NMA) of the conformational transition of the homotrimer AniA structure. The motion of the combined four lowest normal modes of vibrations described the opening and closing states of cupredoxin domain II (Cu^{2+} catalytic active site) of the AniA structure. Thus, NMA revealed the tendency of the protein to move in a certain direction, even though this movement was not fully explored during the MD simulations. The view on the top of the catalytic active site of the AniA structure shows that the flexibility of the protein is well oriented and can dramatically change the accessible area of the catalytic metal ion Cu^{2+} and its potential interaction with a ligand (NO_2 or peptide). The open state of the homotrimer AniA structure was used to identify several binding pockets. These conformations essentially depended on the sequence of the residue composing the peptide. Afterward, the initial conformation of the peptide (which is in a stable conformation in the solvent) was slightly perturbed during the docking procedure due to the interactions with the receptor.

observed that the Tyr side chains (underlined and in bold in the amino acid sequences of the peptides) of the C7-3 (CN**Y**CRLNLW) and 12-5 (KHY**Y**GGDTTTLW) peptides stabilized in the active site by anchoring the Asp137 carboxylate group close to the metal ion (Cu^{2+}), while the side chains of the neighboring residues of the peptides interacted with the residues of the active site. Figures 5 and S3 show that the Tyr side chain fit in the cavity and established a strong van der Waals contact with the hydrophobic residues of the cavity, while the hydroxyl group of the Tyr formed an H bond with the Asp137 residue. Thereafter, several binding conformations of the
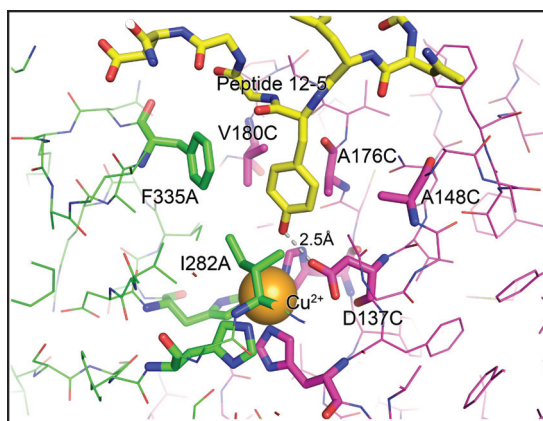

FIG 5 Stick view of the interaction of the peptide 12-5 Tyr side chain in the catalytic active site of AniA homotrimer. The Tyr side chain of the peptide fits in the cavity and established strong van der Waals contact with the hydrophobic residues of the cavity, while the hydroxyl group of the Tyr formed an H bond with the Asp137 residue.

peptides were generated and refined using 10-ns MD simulations in an explicit water model.

The analysis of the binding energy of the peptides in the different pockets showed that the binding free energy of peptides C7-3 and 12-5 in the Cu^{2+} catalytic active site was stronger than that in the other cavities of the protein complex. The calculated relative binding free energy ($\Delta\Delta G$) was > -4 kcal/mol, suggesting that the peptides may bind in the other pockets, but the most important binding pose was in the catalytic domain at the interface of the 2 monomers.

Binding mode of C7-3 and 12-5 in complex with AniA. As displayed in Fig. 6A and B, the two peptides bound in the pocket with distinct conformations. These conformations depended on the peptide's amino acid sequence. Afterward, the initial conformation of the peptide (which had a stable conformation in the solvent) was slightly perturbed during the docking procedure due to interactions with the receptor.

Finally, based on the docked models, we suggested that the residues near the key Tyr side chain should be (i) small to prevent steric clashes throughout the docking of the Tyr side chain into the narrow Cu^{2+} pocket and/or (ii) polar so that they may establish H bonds with the residues on top of the cavity. To validate the peptides' binding prediction and highlight the key residues of the peptides involved in the interactions with the receptor, we performed *in silico* mutations of some specific residues and computed the relative binding free energy of the mutants simulated by MD (Table 2).

Inhibition of AniA nitrite reductase activity by the heptamer and dodecamer peptides. The inhibitory capacity of the two synthesized peptides, C7-3 and 12-5, on the nitrite reductase activity of AniA was assessed in the *in vitro* nitrite consumption assays with DAN. The efficiency of peptide inhibition was calculated from the rate of nitrite reduction in the presence of the peptides at various concentrations (0 to 100 μM). The residual AniA activity (percent inhibition) with the peptides at different concentrations was calculated by comparing the reaction rate of sAniA alone with that of AniA D137A H280A (Fig. 6C). These experiments revealed that peptide 12-5 did not influence the enzymatic activity of AniA (Fig. 6C), and therefore, its additional modifications (Table 2) were not tested. In contrast, C7-3 had a strong inhibitory effect on sAniA with a 50% inhibitory concentration (IC_{50}) of 10.15 μM (Fig. 6C). Next, we tested whether the Tyr side chain plays a role in the C7-3–AniA interaction by measuring nitrite reductase activity in the presence of increasing concentrations of peptides C7-3A and C7-3P, in which the Tyr residue was replaced with Ala and Phe, respectively. The calculated IC_{50}s had values of ~25.18 and >105 μM for C7-3A and C7-3P, respectively, demonstrating that the replacement of Tyr with Phe had detrimental effects on the inhibitor-receptor interaction.

Finally, we also aimed to experimentally verify the effect of the replacement of residues adjacent to Tyr (Cys and Asn) with Ser on the inhibitory potential of C7-3 by including in the nitrite reductase assay peptides C7-3m1 and C7-3m2 (Table 2). The IC_{50}s decreased about 2-fold in comparison to the IC_{50} for C7-3 and were 5.91 and 4.81 μM for C7-3m1 and C7-3m2, respectively (Fig. 6C).

Kinetic analyses of the interaction between AniA and C7-3. Subsequently, biolayer interferometry (BLI) was utilized to study the inhibitory interaction between C7-3 and *N. gonorrhoeae* AniA. BLI is a method of label-free biophysical analysis of small-molecule binding that enables the validation and understanding of primary screening actives and that provides kinetic data similar to those provided by surface plasmon resonance (52, 53). We used a biotinylated C7-3 peptide, C7-3Bio (biotinAhx-ACNYCRLNLWGGGS-NH_2), with 6-aminohexanoic acid (Ahx) being used as a spacer that allowed the peptide to bind to the BLI sensor. First, we verified that the C7-3Bio peptide was active against AniA by assessing the AniA nitrite reductase activity in the presence of increasing concentrations of the peptide. These experiments gave an IC_{50} of 13.47 μM, a value very close to the IC_{50} of the unmodified C7-3 peptide inhibitor (Fig. 6C). Biotinylated C7-3 was immobilized on disposable streptavidin sensors and incubated
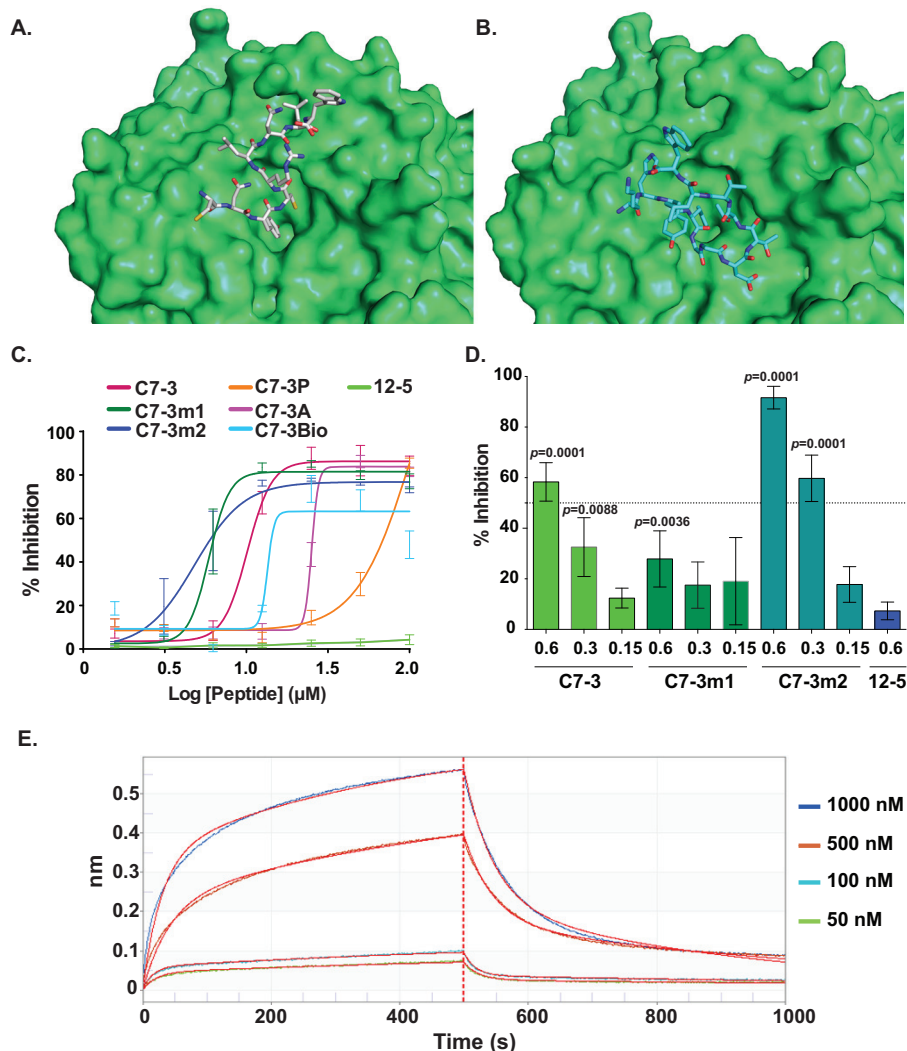
FIG 6 Binding studies. (A, B) Binding mode of C7-3 (A) and 12-5 (B) in the Cu^{2+} active site of the AniA homotrimer. Peptides C7-3 (A) and 12-5 (B) bound in the AniA pocket with distinct conformations. These conformations essentially depended on the sequence of the residues composing the peptide. Afterward, the initial conformation of the peptide (which is in a stable conformation in the solvent) was slightly perturbed during the docking procedure due to the interactions with the receptor. (C) Inhibition of nitrite reductase activity of sAniA. Nitrite reductase inhibition plot of sAniA with synthetic peptides C7-3 and 12-5 and mutated variants of C7-3 (C7-3m1, C7-3m2, C7-3P, and C7-3A). sAniA was preincubated with various concentrations (0 to 100 μM) of synthetic peptides for 1 h at room temperature following measurement of nitrite reductase activity with DAN. Percent inhibition was calculated using the formula $100 \cdot \{1 - [(x - y)/(z - y)]\}$, where x, y, and z are the concentrations of nitrite in samples containing sAniA incubated with synthetic peptides, AniA D137A H280A, and sAniA, respectively. (D) Inhibition of the nitrite reductase activity of intact *N. gonorrhoeae* cells. Inhibition of nitrite reductase AniA was assessed using intact gonococci. Bacteria were preincubated with different concentrations of synthetic peptides (0, 0.6, 0.3, and 0.15 mM) for 1 h, followed by measurement of nitrite reductase activity using DAN. Percent inhibition was calculated using the formula $100 \cdot \{1 - [(x - y)/(z - y)]\}$, where x, y, and z are the concentrations of nitrite in samples containing FA1090 $\Delta aniA/P_{lac}::aniA$ incubated with synthetic peptides, $\Delta aniA/P_{lac}::aniA$ D137A H280A, and $\Delta aniA/P_{lac}::aniA$, respectively. Statistically significant P values are reported. (E) Kinetic analyses of the interaction between AniA and C7-3. The binding affinity between AniA and the C7-3 peptide was measured using biolayer interferometry. The biotinylated C7-3 peptide was immobilized on a streptavidin-coated sensor and incubated with increasing concentrations of recombinant AniA (50 to 1,000 nM). Experiments were repeated on three separate occasions, and the dissociation constants were calculated by globally fitting the curves with 2:1 binding kinetics. The K_D determined for C7-3 was 775 ± 88.5 nM (average ± SEM from three independent experiments).

with increasing concentrations of AniA. The BLI experiments were performed using a steady-state method and curve fitting of the association and dissociation responses. The curves were biphasic, indicating that more than one interaction was occurring, and the 2:1 heterogeneous ligand model gave a calculated K_D (equilibrium dissociation

TABLE 2 *In silico* analysis of $\Delta\Delta G$ of C7-3 and variants simulated by MD interacting in the Cu^{2+} cavity of the AniA homotrimer[a]

Peptide[b]	$\Delta\Delta G$ (kcal/mol)
CNYCRLNLW	0.0
CNY**S**RLNLW	−0.5
C**S**YCRLNLW	−0.8
KHYYGGDTTTLW	0.0
KHYYG**N**DTTTLW	−0.6
KHYYG**S**DTTTLW	−0.9
KHYYGGDTT**S**LW	−0.8
KHYYGG**E**TTTLW	−0.6

[a]To validate the peptide binding prediction and highlight the key residues of the peptides involved in the interactions with the receptor, we mutated *in silico* some specific residues and computed the relative binding free energy of the mutants simulated by MD, where $\Delta\Delta G = \Delta G$ for the mutant $- \Delta G$ for the wild type. The peptides CNYCRLNLW and KHYYGGDTTTLW were wild types and were assigned $\Delta\Delta G$ values of 0.0 kcal/mol.
[b]Boldface amino acids are those that were mutated *in silico*.

constant) value of 775 $\pm$ 88.5 nM, confirming the strong ligand-receptor interaction (Fig. 6E).

Inhibition of AniA nitrite reductase activity of intact *N. gonorrhoeae* cells and MIC$_{50}$ determination. To test whether the C7-3 peptide and its modifications, C7-3m1 and C7-3m2, as well as the 12-5 peptide were capable of blocking the AniA enzymatic activity of intact gonococci, *N. gonorrhoeae* FA1090 $\Delta aniA$/P$_{lac}$::*aniA* and $\Delta aniA$/P$_{lac}$::*aniA* D137A H280A were utilized in nitrite consumption assays as described in Materials and Methods. Incubation of $\Delta aniA$/P$_{lac}$::*aniA* cells, even with the highest tested concentration of 12-5 peptide (0.6 mM), had no effect on AniA activity, whereas the same concentration of C7-3m2 gave 90% inhibition (Fig. 6D). Also, 50% inhibition of nitrite reductase activity was observed with C7-3 and C7-3m2 at concentrations of 0.6 and 0.3 mM, respectively, and C7-3mod1 moderately inhibited AniA.

Finally, we aimed to examine the ability of C7-3, C7-3m1, and C7-3m2 to inhibit *N. gonorrhoeae* growth under anaerobic conditions using a microdilution method in the broth medium established previously for *N. gonorrhoeae* 1291 (31). Despite multiple trials, FA1090 failed to grow under these conditions; therefore, we chose strain 1291 for use in these experiments. The MIC$_{50}$ for both C7-3 and C7-3m2 was 0.6 mM, whereas C7-3mod1 did not exhibit a significant effect on *N. gonorrhoeae* growth.

Altogether, these studies confirmed the C7-3 peptide to be the first identified inhibitor of nitrite reductase with promising inhibitory activity *in vitro*.

DISCUSSION

Antibiotic resistance in *N. gonorrhoeae* continuously challenges treatment and remains a public health concern globally (15, 54, 55). The development of antibacterial compounds with new modes of action, including targeting of nonconventional molecules, is critical in the battle with antibiotic-resistant gonorrhea. AniA has potential as a nonconventional drug target for several reasons: (i) it is a surface-exposed lipoprotein (31), which allows accessibility by a potential inhibitor(s); (ii) it plays a pivotal function in *N. gonorrhoeae* biology, specifically, in the denitrification pathway (Fig. 1A and D) (30) and in biofilm formation (56), and thus, its inhibition could affect slowly growing bacteria, which often hamper antimicrobial therapy (57); (iii) it displays a high level of sequence conservation (see Fig. S2 in the supplemental material) (27) and is expressed by a wide range of contemporary gonococci as well as under various growth conditions relevant to infection (Fig. 2) (36, 44); and (iv) the crystal structures of AniA, particularly the newly solved I4$_1$22 crystals (Fig. 1 and Table 1) (PDB accession number 5UE6) (27), should be amenable for cocrystallization or soaking experiments with potential inhibitors or small-molecule fragments, facilitating drug discovery.

In this study, we applied a phage display approach to identify peptide ligands interacting with AniA (Fig. 3). The phage display technology is a biomolecular tool with applications in basic research and in drug discovery. Ligands identified from the

screening of phage-displayed peptide libraries enabled the selection of peptides with an affinity to biologically relevant sites on the surface of the target protein (47, 58, 59). AniA belongs to the surface-exposed copper nitrite reductases, which are responsible for the reduction of nitrite to nitric oxide under oxygen-limiting conditions and are primarily found in Gram-negative bacteria (27). AniA forms homotrimers via extensive monomer-monomer interactions (Fig. 1B and C) (27). We reasoned that a peptide ligand(s) could interfere with the AniA function either directly, by binding to the active-site cavity, or indirectly, by either preventing AniA oligomerization or disrupting the protein-protein interaction with the neisserial azurin Laz protein, which serves as the electron donor for AniA (60), or with AccA, a periplasmic copper chaperone that delivers Cu to AniA, generating an active nitrite reductase (61). Biopanning experiments with two diverse M13 phage display libraries resulted in the discovery of 29 unique peptides (Fig. 3B). We did not find peptide homologs in the databases, but searches of two databases, the PepBank and SAROTUP databases (62, 63), revealed that none of the identified peptides qualified as target unrelated. The phage-displayed peptides showed different relative binding affinities in the ELISA that did not correspond to the frequency of phage recovery (Fig. 3B and C). For instance, a highly predominant C7-3 peptide, which was identified 19 times, showed about a 2-fold lower relative binding to sAniA than the 12-5 peptide, identified only once. This phenomenon has been observed in other phage display approaches, e.g., against the essential cell division protein FtsA (64). This could be due to multiple reasons, including phage infection and replication efficiency, folding bias, or protein translocation, as well as differences between the conformation of the target resulting from directly coating a plastic surface for ELISA and the conformation resulting from the solution-phase panning with affinity bead capture used in biopanning experiments.

The segments displayed in the Ph.D.-C7C library are flanked by a pair of Cys residues, which are oxidized during phage assembly to a disulfide linkage, resulting in the displayed peptides presenting to the target as loops. We noted, however, that C7-3 contained a mutation at the C terminus of the peptide, where the second Cys residue was replaced with Trp (Fig. 3B), which affected the way that the peptide was presented to the receptor. Phage-displayed peptides with this mutation must have been enclosed in the original Ph.D.-C7C library. Docking studies of two peptides selected for further evaluation, heptameric C7-3 and dodecameric 12-5, showed several possible interactions with the AniA homotrimer (Fig. 4, 5, and 6A and B). Experimental evaluation of these two peptides in biochemical nitrite reductase inhibition assays, whole-cell nitrite consumption assays, and MIC_{50} experiments conducted under anaerobic conditions demonstrated that C7-3 is a promising inhibitor of the AniA nitrite reductase activity (Fig. 6C and D). Finally, the AniA–C7-3 interaction was also confirmed by BLI experiments, in which the K_D was calculated to be in the nanomolar range (Fig. 6E). We speculate that the 12-5 peptide could bind to the sites of AniA that were not critical for AniA nitrite reductase function or were not accessible in the whole-cell assay, for instance, at the AniA-Laz or AniA-AccA interaction sites.

We initiated optimization of C7-3 by experimental verification of the *in silico* alterations of residues adjacent to the key Tyr side chain (Table 2). Of two synthesized derivatives, C7-3m2 showed a promising IC_{50} in a biochemical assay and 90% inhibition of AniA nitrite reductase activity in intact gonococci (Fig. 6C and D), supporting the suggestion that a small and hydrophobic residue adjacent to the key Tyr side chain might enhance the interactions of the peptide ligand with the receptor. However, C7-3m2 showed an MIC_{50} value identical to that of C7-3 (0.6 mM), suggesting lower peptide stability under the tested conditions.

Together, our studies identified the first and potent inhibitor of the pivotal gonococcal surface-exposed protein AniA. The therapeutic utilization of peptides is often limited due to their degradation, low permeability, and unsuitability for oral administration. However, we have discovered a novel structure that may constitute the core for the synthesis of libraries of peptidomimetic molecules. Several lines of evidence presented here suggest that C7-3 inhibits AniA by binding the catalytic active site, and

characterization of the exact mechanism of this interaction, as well as further medicinal chemistry approaches, will require cocrystallization of sAniA with C7-3. In addition, as the C7-3 peptide is directed to the key functional site of AniA, it could potentially be exploited as a surrogate ligand in a campaign of high-throughput screening of diverse small-molecule libraries to identify AniA inhibitors.

MATERIALS AND METHODS

Bacterial strains and growth conditions. *N. gonorrhoeae* FA1090 (65) was cultured as specified in the text on gonococcal base solid medium (GCB; Difco) for 18 to 22 h at 37°C in the presence of a 5% atmospheric CO_2 or anaerobically as described previously (44) or in gonococcal base liquid medium (GCBL) supplemented with sodium bicarbonate at a final concentration of 0.042% and Kellogg's supplement I and II in ratios of 1:100 and 1:1,000, respectively (66). Piliated gonococci were used for DNA transformation, while nonpiliated variants were used in all other experiments. *Escherichia coli* strains either were grown on Luria-Bertani agar (Difco) or were cultured in Luria-Bertani broth (Difco) at 37°C.

Antibiotics were used on selected bacteria at the following concentrations: for *N. gonorrhoeae*, kanamycin was used at 40 μg/ml and erythromycin was used at 0.5 μg/ml, and for *E. coli*, kanamycin was used at 50 μg/ml and erythromycin was used at 250 μg/ml.

Genetic manipulations and site-directed mutagenesis. Oligonucleotides were designed on the basis of the genomic sequence of *N. gonorrhoeae* FA1090 (GenBank accession number NC_002946) using SnapGene software (version 2.8; GSL Biotech LLC) and synthesized by Integrated DNA Technologies. Genomic DNA was isolated with a Wizard genomic DNA purification kit (Promega). PCR products and plasmid DNA were purified using a QIAprep spin miniprep kit (Qiagen). PCRs were performed using chromosomal or plasmid DNA as the template, appropriate oligonucleotides, and Q5 high-fidelity DNA polymerase (NEB). *E. coli* MC1061 was used as the host during the molecular cloning and site-directed mutagenesis. The constructs obtained were verified by Sanger sequencing at the Center for Genomic Research and Biocomputing at Oregon State University. Transformation of *N. gonorrhoeae* was performed as described previously (67).

The clean deletion of *aniA*, resulting in the Δ*aniA* mutant, was constructed in *N. gonorrhoeae* FA1090 by in-frame replacement of *aniA* (*ngo1276*) in its native chromosomal locus with the nonpolar kanamycin resistance cassette using a strategy described by Zielke et al. (44). The constructs for the deletion of *aniA* were obtained using Gibson assembly (68) as described below. The 1-kb upstream DNA region was amplified using oligonucleotides aniA_up_fwd (5'-CCTTAATTAAGTCTAGAGTCGCCGGGACGGTTGGTCGA-3') and aniA_up_rev (5'-CAGCCTACACGCGTTTCATAATGTTTTCCTTTTGTAAGAAAAGTAGGG-3'), and 1 kb downstream from *aniA* was amplified with primers aniA_down_fwd (5'-TAATTCCCATAGCGTTTATTAAATCGGATACCCGTCATTAGC-3') and aniA_down_rev (5'-GCCTGCAGGTTTAAACAGTCGGCAAGGCGAGGCAACGC-3'). The kanamycin resistance cassette was amplified using oligonucleotides aniA_kan_fwd (5'-TATGAAACGCGTGTAGGCTGGAGCTGCT-3') and aniA_kan_rev (5'-AATAAACGCTATGGGAATTAGCCATGGTCC-3'), using pKD4 as a template. The linearized pNEB193 was obtained by PCR amplification using primers pNEB193_fwd (5'-GACTGTTTAAACCTGCAG-3') and pNEB193_rev (5'-GACTCTAGACTTAATTAAGGATCC-3'). All fragments were purified, mixed in equimolar proportions, and assembled using the Gibson assembly master mix. The plasmid obtained, pNEB193-ΔaniA, was linearized with HindIII and introduced into FA1090. Clones were selected on solid medium supplemented with kanamycin and verified by PCR with primers aniA_check_f (5'-CTGTCCCATTTTGAGAGCTCC-3') and aniA_check_r (5'-CCTTGTCGGCGCAATAG-3') and immunoblotting analyses using polyclonal anti-AniA antiserum (67).

For complementation studies, the wild-type *aniA* allele was amplified with primers aniA_pGCC4_f (5'-CTGTTAATTAAAAAAAGGAAAACATTATCAAACGCC-3') and aniA_pGCC4_r (5'-GCTAATGACGGGTATCCGAT-3'). Subsequently, the PCR product was digested with PacI and cloned into the PacI- and PmeI-digested pGCC4 vector under the control of the P_{lac} promoter, and the pGCC4 vector carrying the PCR product was introduced into the chromosome of FA1090 Δ*aniA*, creating the Δ*aniA*/P_{lac}::*aniA* strain.

To generate a construct for overexpression and purification of a mutated, recombinant version of AniA, AniA D137A H280A, site-directed mutagenesis was performed in consecutive reactions using as the template pET28-aniA (36), primer pair D137A-F (5'-CGCACAACGTCGCCTTCCACGCCGCAA-3') and D137A-R (5'-TTGCGGCGTGGAAGGCGACGTTGTGCG-3') and primer pair H280A-F (5'-GAACTTGGTGTCTTCCTTCGCCGTCATCGGCGAAATCTTC-3') and H280A-R (5'-GAAGATTTCGCCGATGACGGCGAAGGAAGACACCAAGTTC-3'), and a Q5 site-directed mutagenesis kit (NEB), per the manufacturer's manual. The presence of mutated sites in the plasmid obtained, pET28-aniAD137A H280A, was confirmed by Sanger sequencing.

To generate pGCC4-aniAD137A H280A, the Gibson assembly method was used to replace wild-type *aniA* with a fragment containing mutated sites. The fragment containing the mutation was amplified using primers RAZ414 (5'-GAACCGCCGGCCAGGCACGATGGTGCTTTGTACGTTTTCGTTAATCAG-3') and RAZ415 (5'-CTACCGCCGAAACGCCTGCAGGCGAACTGCCCG-3') and pET28-aniAD137A H280A as the template. Primers RAZ413 (5'-CGTGCCTGCCGGCCGGTTC-3') and RAZ416 (5'-GCGTTTCGGCGGTAGCTTGTG-3') and plasmid pGCC4-aniA were used to amplify the remaining fragment. Both fragments were gel purified and mixed in equimolar proportions before the Gibson assembly master mix was added (NEB). pGCC4-aniAD137A H280A was introduced into the FA1090 Δ*aniA* chromosome.

Protein purification. Overproduction of recombinant variants of AniA, including a wild-type protein which lacks the N-terminal palmitoylation signal, sAniA (36), as well as mutated AniA, AniA D137A H280A, was performed in *Escherichia coli* BL21(DE3) by addition of IPTG to a final concentration of 0.5 mM when the cultures reached an optical density at 600 nm (OD_{600}) of 0.5. Following 3.5 h of incubation, the

bacteria were pelleted by centrifugation and the pellets were resuspended in lysis buffer (20 mM HEPES, pH 7.5, 500 mM NaCl, 10 mM imidazole) supplemented with a Pierce protease inhibitor minitablet (Thermo Scientific). Cells were lysed by passaging them five times through a French pressure cell at 12,000 lb/in^2. Unbroken cells and cell debris were separated from the soluble protein fraction by centrifugation at 16,000 $\times$ g for 30 min at 4°C. The supernatants obtained were passed through a 0.45-μm-pore-size membrane filter (VWR International) and applied to a nickel affinity column (Profinity IMAC [immobilized metal affinity chromatography]; Bio-Rad). The columns were washed with 8 bed volumes of lysis buffer and elution buffer (20 mM HEPES, pH 7.5, 500 mM NaCl, 250 mM imidazole) at 97:3 (vol/vol), and proteins were eluted with 5 bed volumes of elution buffer. Eluates were subjected to dialysis against 20 mM HEPES, pH 7.5, supplemented with 0.1 mM cupric chloride dihydrate (EMD Chemicals Inc.) twice for 1 h each time and subsequently overnight at 4°C. The purified sAniA and AniA D137A H280A proteins were mixed with 10% glycerol and stored at −80°C.

Crystallization, data collection, and structure solution. Crystallization trials were performed in the vapor diffusion hanging-drop format using a mosquito crystal robot (TTP Labtech). Crystallization solutions from JCSG core suites I to IV (Qiagen) were mixed with the protein solution at three different ratios (0.05 μl protein plus 0.15 μl crystallization solution, 0.1 μl protein plus 0.1 μl crystallization solution, 0.15 μl protein plus 0.05 μl crystallization solution). The initial crystals were harvested without optimization using suitable cryoprotection solutions and flash-cooled in liquid nitrogen. All data were collected at the Southeast Regional Collaborative Access Team (SER-CAT) 22-ID beamline at the Advanced Photon Source, Argonne National Laboratory. The data were processed and scaled using the XDS and XSCALE packages (69).

A 1.90-Å data set in space group P2$_1$2$_1$2$_1$ was collected from a single crystal grown in 0.1 M Tris-HCl, pH 8.5, 2.0 M ammonium dihydrogen phosphate (JCSG Core II-A11). The crystal was cryoprotected in crystallization solution supplemented with 20% glycerol. Initial phases were determined by molecular replacement using Phaser software (70) and the AniA structure (PDB accession number 1KBV) as a search model (27). The model was rebuilt using the Coot program (71) and refined using the Phenix program (72).

A 2.35-Å data set in space group I4$_1$22 was collected from a single crystal grown in 0.2 M potassium thiocyanate, 20% PEG 3350 (JCSG core I-C9) and cryoprotected in crystallization solution supplemented with 20% glycerol. The overall completeness of this data set was 84.8% due to the small crystal size and radiation damage. The structure was solved using Phaser software and the AniA structure in space group P2$_1$2$_1$2$_1$ (PDB accession number 5TB7) as a search model. The structure was corrected using the Coot program and refined using the Phenix program.

The quality of the structures was assessed using Coot and the MolProbity server (http://molprobity .biochem.duke.edu) (73). The structural superpositions were performed using the Dali server (http:// ekhidna2.biocenter.helsinki.fi/dali/) (74). The structural figures were generated using the PyMOL molecular graphics system (version 1.8; Schrödinger, LLC).

Immunoblotting. Expression of AniA was assessed in a panel of geographically, temporally, and genetically diverse *N. gonorrhoeae* isolates, including commonly used laboratory strains FA1090 (65), MS11 (75), 1291 (76), and F62 (77); clinical isolates LGB1, LG2, LG14, LG20, and LGB26, which were collected from two public health clinics in Baltimore, MD, from 1991 to 1994 and differ in their *porB* variable region types and pulsed-field gel electrophoresis patterns (36, 79); 13 isolates from patients attending the Public Health-Seattle & King County, WA, Sexually Transmitted Disease clinic from 2011 to 2013 (the UW strains in Fig. 2) (44); and the 2016 WHO reference strains (46). All strains were cultured concurrently on solid medium collected from GCB plates for 20 h in 5% CO$_2$ at 37°C, and whole-cell lysates were prepared in SDS sample buffer in the presence of 50 mM dithiothreitol, normalized by the number of OD$_{600}$ units, and separated in 4 to 20% mini-Protean TGX precast gels (Bio-Rad). The immunoblotting analysis was performed using polyclonal rabbit antiserum against recombinant AniA (3).

Phage display. To identify peptide ligands interacting with AniA, two M13-based phage libraries, Ph.D.-C7C and Ph.D.-12 (New England BioLabs), were used in biopanning experiments following procedures described in a study reporting on the identification of peptide inhibitors targeting *Clostridium difficile* toxins A and B (80). Magnetic Ni-NTA bead-based affinity capture was used to immobilize sAniA. A preclearance step was included prior to each round of biopanning to remove Ni^{2+} and plastic binders from the phage pool (58, 80). The phages from each library (10^{10} PFU/ml) were incubated with magnetic Ni-NTA agarose beads (250 μg capacity) at room temperature for 1 h. The supernatants of this solution provided the precleared phage pool. For target immobilization, Ni-NTA beads (capacity, 50 μg) were coated with 100 μg of sAniA. Unbound sAniA was washed away, and the precleared phage pool was added. Following incubation, unbound phages were removed by washing 20 times with TBST (50 mM Tris-HCl, pH 8.6, 150 mM NaCl, 0.5% Tween 20). Three rounds of biopanning were performed, with increasing specificity being obtained by raising the Tween 20 concentration from 0.1% in the first biopanning experiment to 0.5% in the subsequent two rounds during the wash step (64, 81). Elution of phages was performed with 0.2 M glycine-HCl (pH 2.2). At the end of each round of selection, eluted phages were titrated and amplified in *E. coli* ER2738 (NEB) per the manufacturer's protocol. After the third round, 24 phage plaques from each library were randomly selected. Phage DNA was purified as recommended in the manufacturer's protocol (NEB) and sequenced using 96 gIII sequencing primer 5′-CCCTCATAGTTAGCGTAACG-3′.

Phage ELISA. Individual wells in 96-well transparent plates (Greiner-Bio) were coated with 100 μl of 100 μg/ml of sAniA suspended in 0.1 M NaHCO$_3$, pH 8.6, and incubated overnight at 4°C in an airtight humidified box. After incubation, excess target solution was shaken out and the wells were filled with 300 μl of blocking buffer (0.1 M NaHCO$_3$, pH 8.6, 5 mg/ml bovine serum albumin). Following 2 h of

incubation at 4°C, the blocking buffer was removed and the wells were washed six times with 200 μl of TBST (50 mM Tris-HCl, pH 8.6, 150 mM NaCl, 0.5% Tween 20). Isolated individual phage amplifications (10^{10} PFU) in 100 μl of TBST were incubated at room temperature for 1 h with rocking. All wells were then cleared by shaking and washed six times with 200 μl of TBST. A solution containing anti-M13 HRP-linked monoclonal antibodies (1:5,000 dilution in blocking buffer; NEB) was distributed at 200 μl per well, and the plate was incubated with rocking at room temperature for 1 h. The wells were washed six times with TBST and incubated by use of Turbo tetramethylbenzidine (TMB)-ELISA substrate for 30 min with rocking at room temperature. To stop the reaction, 100 μl of 1.78 M H_2SO_4 was added to each well. A Synergy HT plate reader (BioTek) measured the color intensity, and readings were compared to those in the control wells, which underwent a treatment that was identical to that described above but that lacked sAniA (designated the control), and to the signal from wild-type infectious virions that did not display peptides, wild-type phage M13KE (10^{10} PFU; designated the wild type), derived from the phage display cloning vector (NEB). Data from seven independent experiments are shown as means and standard errors of the means (SEMs).

Measurements of nitrite reductase activity with purified AniA variants. Enzymatic activity assessments with sAniA and AniA D137A H280A were performed on the basis of previous work (27, 41), but a highly sensitive fluorometric assay for nitrite measurements that relies on the reaction of nitrite with 2,3-diaminonaphthalene (DAN) to form the fluorescent product, 1-(H)-naphthotriazole, was used (42). All reactions were conducted under anoxic or microoxic conditions. Fluorescence was measured at an excitation wavelength of 360/40 nm and an emission wavelength of 460/40 nm at a gain of 50 using a Synergy HT plate reader (BioTek). The sAniA and AniA D137A H280A activities are expressed as the mean reaction rate (nanomoles of nitrite reduced per minute per microgram of protein) from at least 10 independent experiments over the course of a nitrite utilization assay (31).

Determination of peptide inhibitory concentrations. Synthetic peptides 12-5 (H-KHYYGGDTTTL WGGGS-NH$_2$), C7-3 (H-ACNYCRLNLWGGGS-NH$_2$), C7-3m1 (H-ACNYSRLNLWGGGS-NH$_2$), C7-3m2 (H-ACSY CRLNLWGGGS-NH$_2$), C7-3P (H-ACNFCRLNLWGGGS-NH$_2$), C7-3A (H-ACNACRLNLWGGGS-NH$_2$), and C7-3Bio, which is a version of C7-3 biotinylated at the N terminus (biotinAhx-ACNYCRLNLWGGGS-NH$_2$), were acquired from Pepmic Co., dissolved in double-distilled H_2O or dimethylformamide, and serially diluted before addition to sAniA (1 μM). Nitrite measurements with DAN were performed as described above after preincubation of samples for 1 h at room temperature. Control reactions consisted of sAniA alone and AniA D137A H280A, treated in the same manner as the experimental samples. Reactions were performed in at least 12 independent experiments. Percent inhibition was calculated using the formula $100 \cdot \{1 - [(x - y)/(z - y)]\}$, where x, y, and z are the concentrations of nitrite in samples containing sAniA incubated with synthetic peptides, AniA D137A H280A, and sAniA, respectively. The data were analyzed with a nonlinear log(inhibitor)-versus-response-variable slope (four-parameter) curve-fitting technique (GraphPad) to obtain IC_{50}s. All experiments were performed in at least 10 independent trials.

Whole-cell nitrite utilization studies. *N. gonorrhoeae* FA1090 $\Delta aniA$/P$_{lac}$::*aniA* and $\Delta aniA$/P$_{lac}$::D137A H280A were grown to an OD_{600} of $\sim$1.0, gently spun down, decanted, and resuspended in GCBL. Cell suspensions were incubated in the absence or presence of synthetic peptides 12-5, C7-3, C7-3m1, and C7-3m2 (0.15, 0.3, and 0.6 mM) at 37°C for 30 min. Subsequently, 0.1 mM sodium nitrite was added and the samples were transferred into an anaerobic chamber. After 1 h, nitrite consumption was measured using the Griess reagent (Biotium) as previously described for an *N. gonorrhoeae* nitrite reductase whole-cell assay (31). Absorbance (OD_{545}) values were measured using a Synergy HT plate reader (BioTek), and the nitrite concentration was assessed against a nitrite standard prepared in GCBL. Percent inhibition was calculated using the formula $100 \cdot \{1 - [(x - y)/(z - y)]\}$, where x, y, and z are the concentrations of nitrite in samples containing FA1090 $\Delta aniA$/P$_{lac}$::*aniA* incubated with synthetic pep-tides, $\Delta aniA$/P$_{lac}$::*aniA* D137A H280A, and $\Delta aniA$/P$_{lac}$::*aniA*, respectively. Experiments were performed on at least three separate occasions, and means with SEMs are reported.

Determination of MIC$_{50}$. *N. gonorrhoeae* 1291 (82) cells were grown on GCB for 18 to 22 h at 37°C in the presence of 5% atmospheric CO_2. Bacteria were inoculated into GCBL supplemented with 0.042% sodium bicarbonate and incubated with shaking at 37°C for 3 h. Then, the culture was diluted to a concentration of approximately 5×10^5 CFU/ml in brain heart infusion (BHI) broth supplemented with 10% (vol/vol) Levinthal's base, 1% (vol/vol) IsoVitaleX, and 2 mM sodium nitrite (31) containing serially diluted synthetic peptides C7-3, C7-3m1, and C7-3m2. Cultures were incubated anaerobically at 37°C for 18 h, serially diluted, and spotted onto GCB for CFU enumeration. The MIC$_{50}$ was defined as the minimum concentration of the peptide that reduced the mean number of CFU by 50% in comparison to that for the vehicle (dimethyl sulfoxide)-treated culture. Experiments were performed in biological triplicate.

Open state of AniA homotrimer structure. Normal mode analysis (NMA) is a method for charac-terizing the motions of macromolecules based on basis vectors (normal modes), which describes the flexibility of the molecule (83–85). The visual inspection of the 20 lowest-frequency normal modes computed by the elNémo server showed that the first four lowest frequencies of the normal mode of vibrations corresponded to the largest-amplitude motions of the extended and collapsed conformations of the AniA structure (86, 87). Therefore, these modes were used for generating alternative conforma-tional transitions of the protein. To generate alternate conformations of AniA, we started from the structure of AniA in the P2$_1$2$_1$2$_1$ space group (PDB accession number 5TB7) and displaced the protein along the subspace defined by the first low-frequency mode. Such movements were made to generate a more extended state transition (conformation) of the whole structure. Next, the resulting protein conformation defined by the amplitude of variation was energy minimized. The resulting structure was then submitted to the elNémo server, the normal modes were computed, and the protein was displaced

again using the second-lowest new normal mode. This process was repeated until the protein structure was opened using the fourth-lowest normal mode.

Molecular modeling of peptide binding with AniA. The multiple conformational states of the peptides were generated using OMEGA software (Open Eye Scientific Software) and molecular dynamics (MD) simulations (88). The docking poses of the multiconformations of peptide structures (ligands) were performed using 4Dshape+ software (Chem Design Solutions LLC) (89, 90). The docking strategy exhaustively docked/scored all possible positions of each ligand (each peptide conformation) in the AniA binding site. The rigid docking roughly consisted of two steps: shape fitting and application of optimization filters. During the shape fitting, the ligand (peptide structure) was placed into a 0.5-Å-resolution grid box encompassing all active-site atoms (including hydrogen atoms) using the smooth Gaussian potential. Two optimization filters were subsequently processed: rigid-body optimization and optimization of the ligand pose in the dihedral angle space. The pose ensemble was filtered to reject poses that did not have sufficient shape complementarity with the active site of the protein. In separate docking runs, the binding poses of the ligand structure were refined by MD simulations followed by free energy calculations using the Sander module from the Amber12 package (91) as previously described (92–95). The AniA-peptide binding complex was neutralized by adding appropriate counterions and was solvated in a rectangular box of TIP3P (transferable intermolecular potential with 3-points model) water molecules with a minimum solute wall distance of 10 Å (96). The solvated systems were energy minimized and carefully equilibrated. These systems were gradually heated from a temperature of 10 K to one of 298.15 K in 50 ps before an MD simulation was run. The MD simulations were performed with a periodic boundary condition in the NPT ensemble (ensemble in which number of atoms, pressure, and temperature are constant) at a temperature of 298.15 K with Berendsen temperature coupling and a constant pressure (pressure, 1 atm) with isotropic molecule-based scaling. A time step of 2.0 fs was used, with a cutoff of 12 Å being used for the nonbonded interactions, and the SHAKE algorithm was employed to keep all bonds involving hydrogen atoms rigid (97). Long-range interactions were handled using the particle mesh Ewald (PME) algorithm (98). During the energy minimization and MD simulations, only the ligand (peptide) and residue side chains in the binding pocket were permitted to move. We used this constraint to prevent any changes in the AniA structure due to the presence of residues in the loops on the top of the protein active site. A residue-based cutoff of 12 Å was utilized for noncovalent interactions. MD simulations were then carried out for ~10.0 ns. During the simulations, the coordinates of the system were collected every 1 ps. The last 20 snapshots of the simulated structure of the MD trajectory were used to perform the binding free energy calculations.

Binding free energy calculation. The stable MD trajectory obtained for each AniA-peptide complex was used to estimate the binding free energy (ΔG_{bind}) by using the Sietraj program (99). The program calculates the solvated interactions energies (SIE) using five terms and three parameters that were fitted to reproduce the binding free energies of a data set of 99 ligand protein complexes by Naim et al. (99). Sietraj is a substitute for the molecular mechanism/Poisson-Boltzmann surface area (MM/PBSA) method (100).

Biolayer interferometry. The binding affinity of C7-3Bio, a biotinylated C7-3 peptide (biotinAhx-ACNYCRLNLWGGGS-NH$_2$), to sAniA was assessed by biolayer interferometry on an OctetRed 96 system (ForteBio, Menlo Park, CA). C7-3 was first dissolved in dimethylformamide to a final concentration of 1.2 mM and finally in kinetic buffer (ForteBio) to a final concentration of 20 μg/ml. Streptavidin (SA) biosensors (ForteBio) were loaded with C7-3Bio peptides for 10 min. Unloaded tips were used as a control. The sAniA samples were prepared in kinetic buffer at concentrations of 50, 100, 500, and 1,000 nM. The baseline was established for 240 s, and the association and dissociation steps were performed for 500 s. Experiments were performed in three biological replicates with curve fitting using a 2:1 (heterogeneous ligand) model, and K_D value calculations were completed using Octet data analysis software (version 9).

Statistical analyses. Statistical analyses were performed using one-way analysis of variance followed by Dunnett's multiple-comparison test with GraphPad Prism software (version 6). Differences were considered significant when P was <0.05.

Accession number(s). The PDB accession numbers of the newly solved P2$_1$2$_1$2$_1$ and I4$_1$22 crystals are 5TB7 and 5UE6, respectively.

SUPPLEMENTAL MATERIAL

Supplemental material for this article may be found at https://doi.org/10.1128/AAC .00186-17.

SUPPLEMENTAL FILE 1, PDF file, 0.2 MB.

ACKNOWLEDGMENTS

REFERENCES

1. Newman L, Rowley J, Vander Hoorn S, Wijesooriya NS, Unemo M, Low N, Stevens G, Gottlieb S, Kiarie J, Temmerman M. 2015. Global estimates of the prevalence and incidence of four curable sexually transmitted infections in 2012 based on systematic review and global reporting. PLoS One 10:e0143304. https://doi.org/10.1371/journal.pone.0143304.

2. Fleming DT, Wasserheit JN. 1999. From epidemiological synergy to public health policy and practice: the contribution of other sexually transmitted diseases to sexual transmission of HIV infection. Sex Transm Infect 75:3–17. https://doi.org/10.1136/sti.75.1.3.

3. Edwards JL, Apicella MA. 2004. The molecular mechanisms used by Neisseria gonorrhoeae to initiate infection differ between men and women. Clin Microbiol Rev 17:965–981. https://doi.org/10.1128/CMR.17.4.965-981.2004.

4. Woods CR. 2005. Gonococcal infections in neonates and young children. Semin Pediatr Infect Dis 16:258–270. https://doi.org/10.1053/j.spid.2005.06.006.

5. Campbell MF. 1928. The surgical pathology of epididymitis. Ann Surg 88:98–111. https://doi.org/10.1097/00000658-192807000-00012.

6. Westrom LV. 1994. Sexually transmitted diseases and infertility. Sex Transm Dis 21:S32–S37.

7. Ohnishi M, Golparian D, Shimuta K, Saika T, Hoshina S, Iwasaku K, Nakayama S, Kitawaki J, Unemo M. 2011. Is Neisseria gonorrhoeae initiating a future era of untreatable gonorrhea?: detailed characterization of the first strain with high-level resistance to ceftriaxone. Antimicrob Agents Chemother 55:3538–3545. https://doi.org/10.1128/AAC.00325-11.

8. Yokoi S, Deguchi T, Ozawa T, Yasuda M, Ito S, Kubota Y, Tamaki M, Maeda S. 2007. Threat to cefixime treatment for gonorrhea. Emerg Infect Dis 13:1275–1277.

9. Unemo M, Shipitsyna E, Domeika M. 2010. Recommended antimicrobial treatment of uncomplicated gonorrhoea in 2009 in 11 East European countries: implementation of a Neisseria gonorrhoeae antimicrobial susceptibility programme in this region is crucial. Sex Transm Infect 86:442–444. https://doi.org/10.1136/sti.2010.042317.

10. Ison CA, Hussey J, Sankar KN, Evans J, Alexander S. 2011. Gonorrhoea treatment failures to cefixime and azithromycin in England, 2010. Euro Surveill 16(14):pii=19833. http://www.eurosurveillance.org/ViewArticle.aspx?ArticleId=19833.

11. Allen VG, Mitterni L, Seah C, Rebbapragada A, Martin IE, Lee C, Siebert H, Towns L, Melano RG, Low DE. 2013. Neisseria gonorrhoeae treatment failure and susceptibility to cefixime in Toronto, Canada. JAMA 309:163–170. https://doi.org/10.1001/jama.2012.176575.

12. Tapsall J, Read P, Carmody C, Bourne C, Ray S, Limnios A, Sloots T, Whiley D. 2009. Two cases of failed ceftriaxone treatment in pharyngeal gonorrhoea verified by molecular microbiological methods. J Med Microbiol 58:683–687. https://doi.org/10.1099/jmm.0.007641-0.

13. Unemo M, Nicholas RA. 2012. Emergence of multidrug-resistant, extensively drug-resistant and untreatable gonorrhea. Future Microbiol 7:1401–1422. https://doi.org/10.2217/fmb.12.117.

14. Ison CA, Deal C, Unemo M. 2013. Current and future treatment options for gonorrhoea. Sex Transm Infect 89(Suppl 4):iv52–iv56. https://doi.org/10.1136/sextrans-2012-050913.

15. Unemo M, Shafer WM. 2014. Antimicrobial resistance in Neisseria gonorrhoeae in the 21st century: past, evolution, and future. Clin Microbiol Rev 27:587–613. https://doi.org/10.1128/CMR.00010-14.

16. Smith LDS. 1975. The pathogenic anaerobic bacteria, 2nd ed. Charles C Thomas Publisher, Springfield, IL.

17. Short HB, Clark VL, Kellogg DS, Jr, Young FE. 1982. Anaerobic survival of clinical isolates and laboratory strains of Neisseria gonorrhoeae: use in transfer and storage. J Clin Microbiol 15:915–919.

18. Knapp JS, Clark VL. 1984. Anaerobic growth of Neisseria gonorrhoeae coupled to nitrite reduction. Infect Immun 46:176–181.

19. Whitehead RN, Overton TW, Snyder LA, McGowan SJ, Smith H, Cole JA, Saunders NJ. 2007. The small FNR regulon of Neisseria gonorrhoeae: comparison with the larger Escherichia coli FNR regulon and interaction with the NarQ-NarP regulon. BMC Genomics 8:35. https://doi.org/10.1186/1471-2164-8-35.

20. Isabella VM, Clark VL. 2011. Deep sequencing-based analysis of the anaerobic stimulon in Neisseria gonorrhoeae. BMC Genomics 12:51. https://doi.org/10.1186/1471-2164-12-51.

21. Falsetta ML, Bair TB, Ku SC, Vanden Hoven RN, Steichen CT, McEwan AG, Jennings MP, Apicella MA. 2009. Transcriptional profiling identifies the metabolic phenotype of gonococcal biofilms. Infect Immun 77:3522–3532. https://doi.org/10.1128/IAI.00036-09.

22. Phillips NJ, Steichen CT, Schilling B, Post DM, Niles RK, Bair TB, Falsetta ML, Apicella MA, Gibson BW. 2012. Proteomic analysis of Neisseria gonorrhoeae biofilms shows shift to anaerobic respiration and changes in nutrient transport and outermembrane proteins. PLoS One 7:e38303. https://doi.org/10.1371/journal.pone.0038303.

23. Steichen CT, Cho C, Shao JQ, Apicella MA. 2011. The Neisseria gonorrhoeae biofilm matrix contains DNA, and an endogenous nuclease controls its incorporation. Infect Immun 79:1504–1511. https://doi.org/10.1128/IAI.01162-10.

24. Costerton JW, Stewart PS, Greenberg EP. 1999. Bacterial biofilms: a common cause of persistent infections. Science 284:1318–1322. https://doi.org/10.1126/science.284.5418.1318.

25. Fux CA, Costerton JW, Stewart PS, Stoodley P. 2005. Survival strategies of infectious biofilms. Trends Microbiol 13:34–40. https://doi.org/10.1016/j.tim.2004.11.010.

26. Hoiby N, Bjarnsholt T, Givskov M, Molin S, Ciofu O. 2010. Antibiotic resistance of bacterial biofilms. Int J Antimicrob Agents 35:322–332. https://doi.org/10.1016/j.ijantimicag.2009.12.011.

27. Boulanger MJ, Murphy ME. 2002. Crystal structure of the soluble domain of the major anaerobically induced outer membrane protein (AniA) from pathogenic Neisseria: a new class of copper-containing nitrite reductases. J Mol Biol 315:1111–1127. https://doi.org/10.1006/jmbi.2001.5251.

28. Mellies J, Jose J, Meyer TF. 1997. The Neisseria gonorrhoeae gene aniA encodes an inducible nitrite reductase. Mol Gen Genet 256:525–532. https://doi.org/10.1007/s004380050597.

29. Householder TC, Fozo EM, Cardinale JA, Clark VL. 2000. Gonococcal nitric oxide reductase is encoded by a single gene, norB, which is required for anaerobic growth and is induced by nitric oxide. Infect Immun 68:5241–5246. https://doi.org/10.1128/IAI.68.9.5241-5246.2000.

30. Barth KR, Isabella VM, Clark VL. 2009. Biochemical and genomic analysis of the denitrification pathway within the genus Neisseria. Microbiology 155:4093–4103. https://doi.org/10.1099/mic.0.032961-0.

31. Shewell LK, Ku SC, Schulz BL, Jen FE, Mubaiwa TD, Ketterer MR, Apicella MA, Jennings MP. 2013. Recombinant truncated AniA of pathogenic Neisseria elicits a non-native immune response and functional blocking antibodies. Biochem Biophys Res Commun 431:215–220. https://doi.org/10.1016/j.bbrc.2012.12.132.

32. Turner S, Reid E, Smith H, Cole J. 2003. A novel cytochrome c peroxidase from Neisseria gonorrhoeae: a lipoprotein from a Gram-negative bacterium. Biochem J 373:865–873. https://doi.org/10.1042/bj20030088.

33. Turner SM, Moir JW, Griffiths L, Overton TW, Smith H, Cole JA. 2005.

Mutational and biochemical analysis of cytochrome c′, a nitric oxide-binding lipoprotein important for adaptation of Neisseria gonorrhoeae to oxygen-limited growth. Biochem J 388:545–553. https://doi.org/10.1042/BJ20041766.

34. Clark VL, Knapp JS, Thompson S, Klimpel KW. 1988. Presence of antibodies to the major anaerobically induced gonococcal outer membrane protein in sera from patients with gonococcal infections. Microb Pathog 5:381–390. https://doi.org/10.1016/0882-4010(88)90038-1.

35. Jerse AE, Bash MC, Russell MW. 2014. Vaccines against gonorrhea: current status and future challenges. Vaccine 32:1579–1587. https://doi.org/10.1016/j.vaccine.2013.08.067.

36. Zielke RA, Wierzbicki IH, Weber JV, Gafken PR, Sikora AE. 2014. Quantitative proteomics of the Neisseria gonorrhoeae cell envelope and membrane vesicles for the discovery of potential therapeutic targets. Mol Cell Proteomics 13:1299–1317. https://doi.org/10.1074/mcp.M113.029538.

37. Murphy ME, Turley S, Adman ET. 1997. Structure of nitrite bound to copper-containing nitrite reductase from Alcaligenes faecalis. Mechanistic implications. J Biol Chem 272:28455–28460.

38. Ellis MJ, Dodd FE, Strange RW, Prudencio M, Sawers G, Eady RR, Hasnain SS. 2001. X-ray structure of a blue copper nitrite reductase at high pH and in copper-free form at 1.9 A resolution. Acta Crystallogr D Biol Crystallogr 57:1110–1118. https://doi.org/10.1107/S0907444901008654.

39. Liu SQ, Chang T, Liu MY, LeGall J, Chang WC, Zhang JP, Liang DC, Chang WR. 2003. Crystal structure of a NO-forming nitrite reductase mutant: an analog of a transition state in enzymatic reaction. Biochem Biophys Res Commun 302:568–574. https://doi.org/10.1016/S0006-291X(03)00166-9.

40. Cardinale JA, Clark VL. 2000. Expression of AniA, the major anaerobically induced outer membrane protein of Neisseria gonorrhoeae, provides protection against killing by normal human sera. Infect Immun 68:4368–4369. https://doi.org/10.1128/IAI.68.7.4368-4369.2000.

41. Kakutani T, Watanabe H, Arima K, Beppu T. 1981. A blue protein as an inactivating factor for nitrite reductase from Alcaligenes faecalis strain S-6. J Biochem 89:463–472. https://doi.org/10.1093/oxfordjournals.jbchem.a133221.

42. Misko TP, Schilling RJ, Salvemini D, Moore WM, Currie MG. 1993. A fluorometric assay for the measurement of nitrite in biological samples. Anal Biochem 214:11–16. https://doi.org/10.1006/abio.1993.1449.

43. Kakutani T, Watanabe H, Arima K, Beppu T. 1981. Purification and properties of a copper-containing nitrite reductase from a denitrifying bacterium, Alcaligenes faecalis strain S-6. J Biochem 89:453–461. https://doi.org/10.1093/oxfordjournals.jbchem.a133220.

44. Zielke RA, Wierzbicki IH, Baarda BI, Gafken PR, Soge OO, Holmes KK, Jerse AE, Unemo M, Sikora AE. 2016. Proteomics-driven antigen discovery for development of vaccines against gonorrhea. Mol Cell Proteomics 15:2338–2355. https://doi.org/10.1074/mcp.M116.058800.

45. Clark VL, Campbell LA, Palermo DA, Evans TM, Klimpel KW. 1987. Induction and repression of outer membrane proteins by anaerobic growth of Neisseria gonorrhoeae. Infect Immun 55:1359–1364.

46. Unemo M, Golparian D, Sanchez-Buso L, Grad Y, Jacobsson S, Ohnishi M, Lahra MM, Limnios A, Sikora AE, Wi T, Harris SR. 2016. The novel 2016 WHO Neisseria gonorrhoeae reference strains for global quality assurance of laboratory investigations: phenotypic, genetic and reference genome characterization. J Antimicrob Chemother 71:3096–3108. https://doi.org/10.1093/jac/dkw288.

47. Huang JX, Bishop-Hurley SL, Cooper MA. 2012. Development of anti-infectives using phage display: biological agents against bacteria, viruses, and parasites. Antimicrob Agents Chemother 56:4569–4582. https://doi.org/10.1128/AAC.00567-12.

48. Fjell CD, Hiss JA, Hancock RE, Schneider G. 2011. Designing antimicrobial peptides: form follows function. Nat Rev Drug Discov 11:37–51.

49. Petrone P, Pande VS. 2006. Can conformational change be described by only a few normal modes? Biophys J 90:1583–1593. https://doi.org/10.1529/biophysj.105.070045.

50. Stambouli N, Wei NN, Jlizi A, Aissa S, Abdelmalek R, Kilani B, Slim A, Tiouiri BA, Dridi M, Hamza A, Ben Ammar Elgaied A. 2014. Structural insight into a novel human CCR5-V130I variant associated with resistance to HIV-1 infection. J Biomol Struct Dyn 32:1202–1210. https://doi.org/10.1080/07391102.2013.819297.

51. Wei NN, Hamza A, Hao C, Johnson-Scalise T, Xiu Z, Naftolin F, Zhan CG. 2013. Protein flexibility and conformational states of Leishmania antigen eIF-4A: identification of a novel plausible protein adjuvant using

comparative genomics and molecular modeling. J Biomol Struct Dyn 31:841–853. https://doi.org/10.1080/07391102.2012.713781.

52. Concepcion J, Witte K, Wartchow C, Choo S, Yao D, Persson H, Wei J, Li P, Heidecker B, Ma W, Varma R, Zhao LS, Perillat D, Carricato G, Recknor M, Du K, Ho H, Ellis T, Gamez J, Howes M, Phi-Wilson J, Lockard S, Zuk R, Tan H. 2009. Label-free detection of biomolecular interactions using BioLayer interferometry for kinetic characterization. Comb Chem High Throughput Screen 12:791–800. https://doi.org/10.2174/138620709789104915.

53. Shah NB, Duncan TM. 2014. Bio-layer interferometry for measuring kinetics of protein-protein interactions and allosteric ligand effects. J Vis Exp 18:e51383. https://doi.org/10.3791/51383.

54. World Health Organization. 2012. Global action plan to control the spread and impact of antimicrobial resistance in Neisseria gonorrhoeae. World Health Organization, Geneva, Switzerland.

55. Centers for Disease Control and Prevention. 2013. Antibiotic resistance threats in the United States, 2013. Centers for Disease Control and Prevention, U.S. Department of Health and Human Services, Atlanta, GA.

56. Falsetta ML, Steichen CT, McEwan AG, Cho C, Ketterer M, Shao J, Hunt J, Jennings MP, Apicella MA. 2011. The composition and metabolic phenotype of Neisseria gonorrhoeae biofilms. Front Microbiol 2:75. https://doi.org/10.3389/fmicb.2011.00075.

57. Greulich P, Scott M, Evans MR, Allen RJ. 2015. Growth-dependent bacterial susceptibility to ribosome-targeting antibiotics. Mol Syst Biol 11:796. https://doi.org/10.15252/msb.20145949.

58. Molek P, Strukelj B, Bratkovic T. 2011. Peptide phage display as a tool for drug discovery: targeting membrane receptors. Molecules 16:857–887. https://doi.org/10.3390/molecules16010857.

59. Pande J, Szewczyk MM, Grover AK. 2010. Phage display: concept, innovations, applications and future. Biotechnol Adv 28:849–858. https://doi.org/10.1016/j.biotechadv.2010.07.004.

60. Woods JP, Dempsey JF, Kawula TH, Barritt DS, Cannon JG. 1989. Characterization of the neisserial lipid-modified azurin bearing the H.8 epitope. Mol Microbiol 3:583–591. https://doi.org/10.1111/j.1365-2958.1989.tb00205.x.

61. Jen FE, Djoko KY, Bent SJ, Day CJ, McEwan AG, Jennings MP. 2015. A genetic screen reveals a periplasmic copper chaperone required for nitrite reductase activity in pathogenic Neisseria. FASEB J 29:3828–3838. https://doi.org/10.1096/fj.15-270751.

62. Shtatland T, Guettler D, Kossodo M, Pivovarov M, Weissleder R. 2007. PepBank—a database of peptides based on sequence text mining and public peptide data sources. BMC Bioinformatics 8:280. https://doi.org/10.1186/1471-2105-8-280.

63. Huang J, Ru B, Li S, Lin H, Guo FB. 2010. SAROTUP: scanner and reporter of target-unrelated peptides. J Biomed Biotechnol 2010:101932. https://doi.org/10.1155/2010/101932.

64. Paradis-Bleau C, Lloyd A, Sanschagrin F, Clarke T, Blewett A, Bugg TD, Levesque RC. 2008. Phage display-derived inhibitor of the essential cell wall biosynthesis enzyme MurF. BMC Biochem 9:33. https://doi.org/10.1186/1471-2091-9-33.

65. Connell TD, Black WJ, Kawula TH, Barritt DS, Dempsey JA, Kverneland K, Jr, Stephenson A, Schepart BS, Murphy GL, Cannon JG. 1988. Recombination among protein II genes of Neisseria gonorrhoeae generates new coding sequences and increases structural variability in the protein II family. Mol Microbiol 2:227–236. https://doi.org/10.1111/j.1365-2958.1988.tb00024.x.

66. Spence JM, Wright L, Clark VL. 2008. Laboratory maintenance of Neisseria gonorrhoeae. Curr Protoc Microbiol Chapter 4:Unit 4A.1. https://doi.org/10.1002/9780471729259.mc04a01s8.

67. Zielke RA, Gafken PR, Sikora AE. 2014. Quantitative proteomic analysis of the cell envelopes and native membrane vesicles derived from gram-negative bacteria. Curr Protoc Microbiol 34:1F.3.1–1F.3.16. https://doi.org/10.1002/9780471729259.mc01f03s34.

68. Gibson DG, Young L, Chuang RY, Venter JC, Hutchison CA, III, Smith HO. 2009. Enzymatic assembly of DNA molecules up to several hundred kilobases. Nat Methods 6:343–345. https://doi.org/10.1038/nmeth.1318.

69. Kabsch W. 2010. Integration, scaling, space-group assignment and post-refinement. Acta Crystallogr D Biol Crystallogr 66:133–144. https://doi.org/10.1107/S0907444909047374.

70. McCoy AJ, Grosse-Kunstleve RW, Adams PD, Winn MD, Storoni LC, Read RJ. 2007. Phaser crystallographic software. J Appl Crystallogr 40:658–674. https://doi.org/10.1107/S0021889807021206.

71. Emsley P, Lohkamp B, Scott WG, Cowtan K. 2010. Features and development of Coot. Acta Crystallogr D Biol Crystallogr 66:486–501. https://doi.org/10.1107/S0907444910007493.

72. Adams PD, Afonine PV, Bunkoczi G, Chen VB, Davis IW, Echols N, Headd JJ, Hung LW, Kapral GJ, Grosse-Kunstleve RW, McCoy AJ, Moriarty NW, Oeffner R, Read RJ, Richardson DC, Richardson JS, Terwilliger TC, Zwart PH. 2010. PHENIX: a comprehensive Python-based system for macromolecular structure solution. Acta Crystallogr D Biol Crystallogr 66:213–221. https://doi.org/10.1107/S0907444909052925.

73. Chen VB, Arendall WB, III, Headd JJ, Keedy DA, Immormino RM, Kapral GJ, Murray LW, Richardson JS, Richardson DC. 2010. MolProbity: all-atom structure validation for macromolecular crystallography. Acta Crystallogr D Biol Crystallogr 66:12–21. https://doi.org/10.1107/S0907444909042073.

74. Holm L, Laakso LM. 2016. Dali server update. Nucleic Acids Res 44:W351–W355. https://doi.org/10.1093/nar/gkw357.

75. Meyer TF, Mlawer N, So M. 1982. Pilus expression in Neisseria gonorrhoeae involves chromosomal rearrangement. Cell 30:45–52. https://doi.org/10.1016/0092-8674(82)90010-1.

76. Apicella MA, Breen JF, Gagliardi NC. 1978. Degradation of the polysaccharide component of gonococcal lipopolysaccharide by gonococcal and meningococcal sonic extracts. Infect Immun 20:228–234.

77. Sparling PF. 1966. Genetic transformation of Neisseria gonorrhoeae to streptomycin resistance. J Bacteriol 92:1364–1371.

78. Reference deleted.

79. Garvin LE, Bash MC, Keys C, Warner DM, Ram S, Shafer WM, Jerse AE. 2008. Phenotypic and genotypic analyses of Neisseria gonorrhoeae isolates that express frequently recovered PorB PIA variable region types suggest that certain P1a porin sequences confer a selective advantage for urogenital tract infection. Infect Immun 76:3700–3709. https://doi.org/10.1128/IAI.00265-08.

80. Abdeen SJ, Swett RJ, Feig AL. 2010. Peptide inhibitors targeting Clostridium difficile toxins A and B. ACS Chem Biol 5:1097–1103. https://doi.org/10.1021/cb100209b.

81. El Zoeiby A, Sanschagrin F, Darveau A, Brisson JR, Levesque RC. 2003. Identification of novel inhibitors of Pseudomonas aeruginosa MurC enzyme derived from phage-displayed peptide libraries. J Antimicrob Chemother 51:531–543. https://doi.org/10.1093/jac/dkg010.

82. Cohen MS, Cannon JG, Jerse AE, Charniga LM, Isbey SF, Whicker LG. 1994. Human experimentation with Neisseria gonorrhoeae: rationale, methods, and implications for the biology of infection and vaccine development. J Infect Dis 169:532–537. https://doi.org/10.1093/infdis/169.3.532.

83. Tirion MM. 1996. Large amplitude elastic motions in proteins from a single-parameter, atomic analysis. Phys Rev Lett 77:1905–1908. https://doi.org/10.1103/PhysRevLett.77.1905.

84. Hinsen K. 1998. Analysis of domain motions by approximate normal mode calculations. Proteins 33:417–429. https://doi.org/10.1002/(SICI)1097-0134(19981115)33:3<417::AID-PROT10>3.0.CO;2-8.

85. Ma JP. 2004. New advances in normal mode analysis of supermolecular complexes and applications to structural refinement. Current Protein Pept Sci 5:119–123. https://doi.org/10.2174/1389203043486892.

86. Suhre K, Sanejouand YH. 2004. ElNemo: a normal mode web server for protein movement analysis and the generation of templates for molecular replacement. Nucleic Acids Res 32:W610–W614. https://doi.org/10.1093/nar/gkh368.

87. Suhre K, Sanejouand YH. 2004. On the potential of normal-mode analysis for solving difficult molecular-replacement problems. Acta Crystallogr D Biol Crystallogr 60:796–799. https://doi.org/10.1107/S0907444904001982.

88. Hawkins PC, Nicholls A. 2012. Conformer generation with OMEGA: learning from the data set and the analysis of failures. J Chem Infect Model 52:2919–2936. https://doi.org/10.1021/ci300314k.

89. Wei NN, Hamza A. 2014. SABRE: ligand/structure-based virtual screening approach using consensus molecular-shape pattern recognition. J Chem Infect Model 54:338–346. https://doi.org/10.1021/ci4005496.

90. Hamza A, Wagner JM, Wei NN, Kwiatkowski S, Zhan CG, Watt DS, Korotkov KV. 2014. Application of the 4D fingerprint method with a robust scoring function for scaffold-hopping and drug repurposing strategies. J Chem Infect Model 54:2834–2845. https://doi.org/10.1021/ci5003872.

91. Case DA, Darden TA, Cheatham TE, Simmerling CL, Wang J, Duke RE, Luo R, Walker RC, Zhang W, Merz KM, Roberts B, Wang B, Hayik S, Roitberg A, Seabra G, Kolossváry I, Wong KF, Paesani F, Vanicek J, Liu J, Wu X, Brozell SR, Steinbrecher T, Gohlke H, Cai Q, Ye X, Wang J, Hsieh MJ, Cui G, Roe DR, Mathews DH, Seetin MG, Sagui C, Babin V, Luchko T, Gusarov S, Kovalenko A, Kollman PA. 2012. AMBER 12. University of California, San Francisco, CA.

92. Hamza A, Wagner JM, Evans TJ, Frasinyuk MS, Kwiatkowski S, Zhan C-G, Watt DS, Korotkov KV. 2014. Novel mycosin protease MycP1 inhibitors identified by virtual screening and 4D fingerprints. J Chem Infect Model 54:1166–1173. https://doi.org/10.1021/ci500025r.

93. Zhou M, Hamza A, Zhan C-G, Thorson JS. 2013. Assessing the regioselectivity of OleD-catalyzed glycosylation with a diverse set of acceptors. J Nat Prod 76:279–286. https://doi.org/10.1021/np300890h.

94. Zhang W, Sviripa V, Chen X, Shi J, Yu T, Hamza A, Ward ND, Kril LM, Vander Kooi CW, Zhan C-G, Evers BM, Watt DS, Liu C. 2013. Fluorinated N,N-dialkylaminostilbenes repress colon cancer by targeting methionine S-adenosyltransferase 2A. ACS Chem Biol 8:796–803. https://doi.org/10.1021/cb3005353.

95. Hamza A, Zhao X, Tong M, Tai H-H, Zhan C-G. 2011. Novel human mPGES-1 inhibitors identified through structure-based virtual screening. Bioorg Med Chem 19:6077–6086. https://doi.org/10.1016/j.bmc.2011.08.040.

96. Jorgensen WI. 1981. Transferable intermolecular potential functions for water, alcohols, and ethers. Application to liquid water. J Am Chem Soc 103:335–340.

97. Ryckaert J-P, Ciccotti G, Berendsen HJC. 1977. Numerical integration of the Cartesian equations of motion of a system with constraints: molecular dynamics of n-alkanes. J Comput Phys 23:327–341. https://doi.org/10.1016/0021-9991(77)90098-5.

98. Darden T, York D, Pedersen L. 1993. Particle mesh Ewald: an N-log(N) method for Ewald sums in large systems. J Chem Phys 98:10089–10092. https://doi.org/10.1063/1.464397.

99. Naim M, Bhat S, Rankin KN, Dennis S, Chowdhury SF, Siddiqi I, Drabik P, Sulea T, Bayly CI, Jakalian A, Purisima EO. 2007. Solvated interaction energy (SIE) for scoring protein-ligand binding affinities. 1. Exploring the parameter space. J Chem Inf Model 47:122–133.

100. Kollman PA, Massova I, Reyes C, Kuhn B, Huo S, Chong L, Lee M, Lee T, Duan Y, Wang W, Donini O, Cieplak P, Srinivasan J, Case DA, Thomas E, Cheatham I. 2000. Calculating structures and free energies of complex molecules: combining molecular mechanics and continuum models. Acc Chem Res 33:889–897. https://doi.org/10.1021/ar000033j.

101. Karplus PA, Diederichs K. 2012. Linking crystallographic model and data quality. Science 336:1030–1033. https://doi.org/10.1126/science.1218231.

102. Kabsch W. 2010. XDS. Acta Crystallogr D Biol Crystallogr 66:125–132. https://doi.org/10.1107/S0907444909047337.